FORCE CONTROL OF A HYDRAULIC SERVO SYSTEM

A Thesis presented to the Faculty of the Graduate School
University of Missouri

In partial Fulfillment
Of the Requirements for the Degree

Master of Science

---

by
JOSEPH L. KENNEDY

Dr. Roger Fales, Thesis Supervisor

MAY 2009

The undersigned, appointed by the Dean of the Graduate School, have examined the thesis entitled

FORCE CONTROL OF A HYDRAULIC
SERVO SYSTEM

Presented by Joseph L. Kennedy

A candidate for the degree of Master of Science

And hereby certify that in their opinion it is worthy of acceptance.

_____
Dr. Roger Fales

_____
Dr. Noah Mannring

_____
Dr. William Jacoby

…To my father, Jerry Lee Kennedy

ACKNOWLEDGEMENTS

I would like to thank Dr. Roger Fales for his contribution to my research. Dr. Fales introduced me to control systems as an undergraduate at MU and assisted me throughout my Master's program. My Master's thesis would not have been possible without his influence and participation. I would also like to thank Dr. Noah Manring for introducing me to hydraulic systems as a undergraduate. Finally, I would like to thanks all of the teachers and faculty in the Mechanical and Aerospace department at MU for making my Master's program so enjoyable.

TABLE OF CONTENTS

LIST OF ILLUSTRATIONS

Figure Page

LIST OF TABLES

LIST OF ABBREVIATIONS

Abbreviation	Meaning
CL	Closed-loop
DAC	Data Acquisition
FFT	Fast Fourier Transformation
LHP	Left Half Plane
MU	Multiplicative Uncertainty
NP	Nominal Performance
NS	Nominal Stability
OL	Open-loop
P	Proportional
PID	Proportional-Integral-Derivative
QFT	Quantitative Feedback Theory
RHP	Right Half Plane
RP	Robust Performance
RS	Robust Stability
SS	Steady state
SSV	Structured Singular Value
TF	Transfer Function

LIST OF SYMBOLS

Symbol	Definition
A	Low frequency performance requirment
A, B, C, D	State-space representation of the shaped plant
A_o	Cross-sectional area within the needle valve
C_d	Volumetric flow rate through needle valve
DC	DC-gain of the servo system
dP_s	Polynomial for the static DC-gain vs. Input Voltage relationship
dP_t	Polynomial for the triangular DC-gain vs. Input Voltage relationship
e	Error signal from closed-loop system
$\dot{e}$	First derivative of the error
$\ddot{e}$	Second derivative of the error
F_a	Actual force output from closed-loop system
F_d	Desired force output from closed-loop system
G	Plant
G_3	3^{rd}-order transfer function of the closed-loop servo responce
G_4	4^{th}-order transfer function of the closed-loop servo responce
G_n	Nominal plant model
$G_{p,d}$	Dynamically perturbed plant model
$G_{p,p}$	Parametrically perturbed plant model
k_{max}	Maximum gain value
k_{min}	Minimum gain value

K.....Controller

K_D.....Derivative gain

K_H.....H_∞ controller

K_{H3} .....H_∞ controller found from the shaped plant $K_{PID}G_3$

K_{H4} .....H_∞ controller found from the shaped plant $K_{PID}G_4$

K_I.....Integral gain

K_P.....P Controller (proportional gain)

K_{PID} .....PID Controller

$K_{PID}G_3$ .....Shaped plant with 3rd-order model

$K_{PID}G_4$ .....Shaped plant with 4th-order model

L .....Any complex matrix

l_I .....Maximum multiplicative uncertainty

M.....High frequency performance requirment

n .....order of the transfer function model

N.....N-matrix

N_{11}, N_{12}, N_{21}, N_{22}.....Elements of the N-matrix

P.....Generalized plant model (P-matrix)

P_{11}, P_{12}, P_{21}, P_{22}.....Elements of the P-matrix

P_A .....Actuator pressure on the side A

P_B .....Actuator pressure on the side B

P_s.....Polynomial for the static input-output relationship

P_{su} .....Supply pressure from hydraulic power unit

P_t ..... Polynomial for the triangular Input Voltage vs. Output Force relationship

Δp ..... Pressure difference across the needle valve

Q ..... Volumetric flow rate through needle valve

r_k ..... Relative magnitude of the gain uncertainty

w_I ..... Dynamic uncertainty transfer function

w_P ..... Performance weight transfer function

Z, X ..... Unique definite solutions to Riccati equations

Δ ..... Any real scalar

Δ_I ..... Any stable transfer function such that $\|\Delta_I\| \leq 1$

Δ_P ..... Fictitious uncertainty block

ζ ..... Damping ratio

θ ..... Time delay in seconds

μ ..... Structured singular value

ρ ..... Hydraulic fluid density

ρ_s ..... Spectral radius (maximum singular value)

$\overline{\sigma}$ ..... Maximum singular value

ω ..... Frequency ranging from 0 to 100 Hz

ω_B ..... Closed-loop bandwidth frequency

ω_B^* ..... Acheivable bandwidth for a linear system with a right-half-plane zero

ω_{BR} ..... Approximate bandwidth requirement

ω_n ..... Natural frequency

ABSTRACT

The objective of this thesis is to model a hydraulic servo system using force control and then improve upon the performance of the model/system through feedback control design. The hydraulic system is first constructed and tested. Experimental data based linear models of the system are found through input-output measurements. The models contain a right-half-plane zero; therefore, a bandwidth limitation is placed on the control design (i.e. the bandwidth frequency of the control system is limited). Three types of controllers (*P*, *PID*, and H_∞) are designed specifically for the linear models. The closed-loop time domain and frequency domain performance of each control system is found and compared for the models and system. Uncertainties and performance weights are finally used in finding the nominal/robust stability and performance.

Chapter 1.

INTRODUCTION

1.1 Force Feedback Control Systems

Hydraulic control valves (such as a servo-valve) are used within hydraulic control systems to accurately regulate the output of the entire system. The valve provides the interface between the hydraulic power unit and the output device, in this case a linear actuator. The control valve has the ability to receive a signal from a control system in order for the output of the system to track a desired input [1]. Using force feedback to control a hydraulic system allows the user to control the force output from a linear actuator by supplying the control system with a desired force reference signal. Controllers are designed specifically for the closed-loop (CL) system to improve performance (i.e. improve the ability of the system to track a given input signal) and stability (i.e. the ability of the system to adjust to uncertainties).

There are many types of controllers that can be implemented into a CL control system, each of which adds different performance characteristics. The process used in this paper for obtaining CL control is as follows. A linear model (linear transfer function) representing the open-loop (OL) frequency domain performance of the servo system is found through analyzing input-output measurements at given operating points over a range of frequencies. A controller is designed specifically for the linear model and then tested on the servo system to find the CL time domain and frequency domain performance of the system. This process is repeated for different linear models and controllers.

Once a control system is designed and tested, the nominal/robust stability and performance of that control system can be found. The nominal stability and performance are found in relation to the nominal plant (i.e. the linear model found from the input-output measurements). The uncertainties within the OL system (both dynamic and parametric) are used in finding a perturbed plant (i.e. the nominal plant plus all perturbations). The perturbed plant is used in evaluating the robust stability and performance of the CL system (a performance weight transfer function is also required in finding robust performance).

1.2 Background Information and Previous Work

Hydraulic actuators have several non-lineararities due mainly to servo-valve flow and pressure characteristics [2]. The method used in this thesis is based on the linearization of the non-linear dynamics of a hydraulic system about given operating points. The stability and performance of a linear control system is, therefore, only achievable at or near the operating points which the controller is designed around. Linear models are commonly used given their relative simplicity and accuracy at a given operating point (point of interest). In order to model a full range of operating points, a different method must be considered. One such method considers non-linear Quantitative Feedback Theory (QFT) where the non-linear plant is replaced with a "family of linear time invariant transfer functions" [2]. The linear transfer functions are based on experimental input-output measurements (the plant models in the this thesis are found through a similar input-output measurement approach). Non-linear QFT robust control methodology can then be used to design a force controller that is of "low-order" and that

can “maintain satisfactory performance against uncertainties” [2]. A second method for modeling an entire system (not just specific operating points) uses Input-Output Feedback Linearization, which requires full state feedback (an observer can be used to estimate states that can not be measured) [3]. In this approach, no particular operating point is used in obtaining a linear model of the system. Therefore, the performance of a given control system is not influenced by its proximity to the set of operating points, which results in better performance over the entire operating range of the system [3]. Either of the control design methods discussed here can be implemented if the linear method does not result in satisfactory performance due to the uncertainties of the system and/or if a wide range of operating points are needed.

Force control on various hydraulic servo systems has been documented. The system given by [4] is used to simulate modern fly-by-wire flight control systems for testing primary fight actuators. In this application, a “high-bandwidth force response” is needed to simulate the aerodynamic loads that are applied to the control surfaces during flight [4]. Uncertainties in structural stiffness and hydraulic plant parameters require a “robust approach to the design of the force control” [4]. Higher bandwidth frequencies correlate to faster response/rise times and improved robustness is associated with increased stability. Therefore, the control system must have a balance between stability and speed of response. By knowing the performance requirements of the desired system, a specific controller can be chosen based on its performance characteristics.

The modeling and control design process outlined by [4] is similar to the process used in this thesis; however, the experimental setup is different. The movement of the main loading actuator is restricted in this thesis. In contrast, [4] allows movement by

connecting the main loading actuator to a secondary actuator via a lever arm. The experimental setup given by [2] also allows actuator movement by connecting the actuator rod to a spring. Obtaining a control system for the case with actuator movement requires slight adjustments to the control design process outlined in this thesis (i.e. a correction to the force demand must be made based on the displacement and/or velocity of the loading actuator). The experimental setup in this thesis also incorporates a needle valve to regulate hydraulic fluid flow between the high and low-pressure side of the actuator. The experimental setups given by [2] and [4] do not have such a capability. Finally, this thesis gives extensive uncertainty analysis on the control systems, while [2] and [4] only focus on control design.

1.3 Goals/Overview

The goals of this thesis are as follows: construct the hydraulic servo system for lab testing, perform lab tests to create a dynamic model of the servo system, quantify performance limitations to find the highest possible theoretical performance (limitations include saturation and pole/zero locations of the model), increase the performance of the system through control design, analyze the time and frequency domain performance of the control systems, and test for nominal/robust stability and performance. Chapter 2 outlines the experimental setup for the mechanical system and data acquisition process along with a description of the input-output characteristics of the system. The dynamic modeling process is given in Chapter 3, and the performance limitations and control design are discussed in Chapter 4. The time and frequency domain performance of each control system are found in Chapter 5, and the nominal/robust stability and performance

are determined in Chapter 6. Chapter 7 is an overview of the findings and also contains suggestions for future work.

Chapter 2.

EXPERIMENTAL SETUP

2.1 Mechanical Setup

A picture and schematic of the hydraulic servo system are shown in Fig. 1 and Fig. 2, respectively. A double-rod actuator (front and rear piston areas are equal) is used as the force output devise. The rear, *B*, actuator rod is enclosed within a protective casing. The front, *A*, actuator rod is connected to a load cell, which in turn is attached to a stiff steel link. The link is bolted to a bracket that is secured to the same I-beam as the actuator, impeding any movement of the actuator rod during loading. Two pressure sensors are placed on either side of the piston to record fluid pressures within the actuator (i.e. P_A and P_B in Fig. 2). A third pressure sensor records the supply pressure, P_{su}, from the hydraulic power unit. The power unit (shown in Fig. 3) uses an electric motor and hydraulic pump to supply the system with a constant P_{su}. A hydraulic line connects side *A* and *B* of the actuator allowing hydraulic fluid to leak from the high to low-pressure side. A needle valve is placed on the leakage line to control the amount of fluid that can be passed from one side of the actuator to the other.

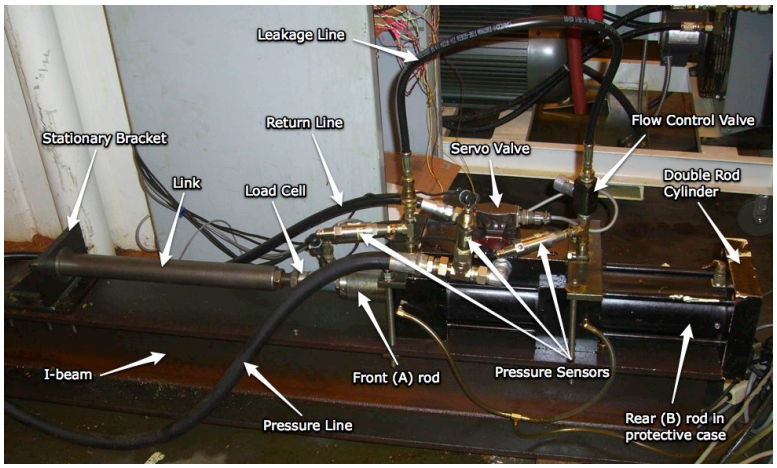

Fig. 1. Hydraulic servo system.

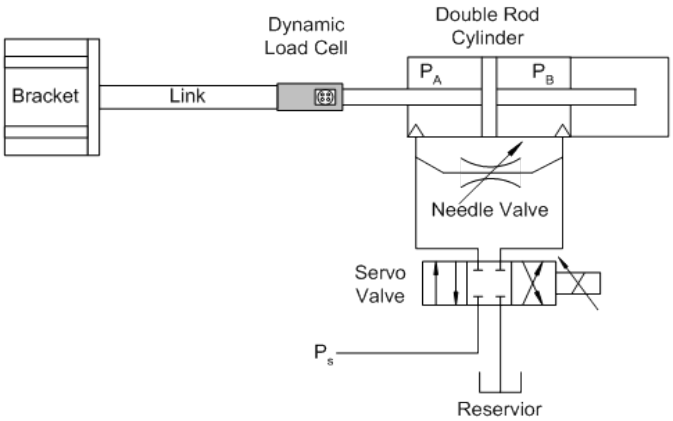

Fig. 2. Schematic of the servo system.

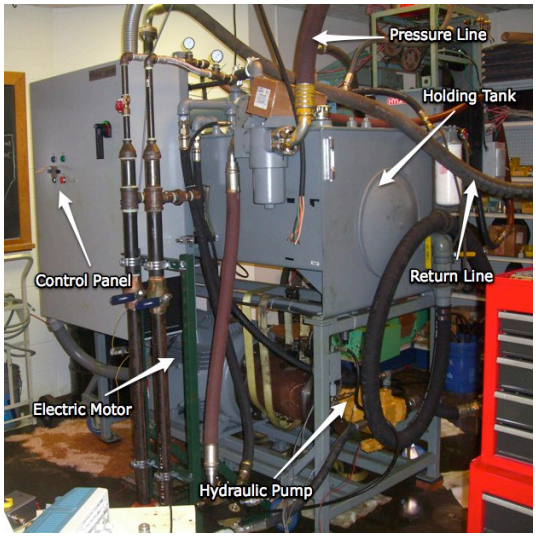

Fig. 3. Hydraulic power unit.

2.2 Data Acquisition Setup

A block diagram of the hydraulic servo system is shown in Fig. 4, and a photo of the electrical equipment is given in Fig. 5. The hydraulic pump supplies the servo-valve/actuator with a constant P_{su}. The PC sends an input voltage signal through an analog output port on the data acquisition (DAC) board where it is converted from a digital-to-analog signal, to the servo amplifier. The input signal is then sent from the amplifier to the servo-valve. A power supply provides the load cell and pressure sensors with a required 20 V. The output voltage from each sensor is sent to the PC through analog input ports on the DAC board where it is converted from an analog-to-digital signal (the output signal from the load cell is passed through an amplifier before it is sent to the DAC board). The load cell signal, along with some type of control system, can then be used to create closed-loop (CL) force control for the system. Simulink® and Matlab® are used as the user interface to generate and analyze all data to and from the PC.

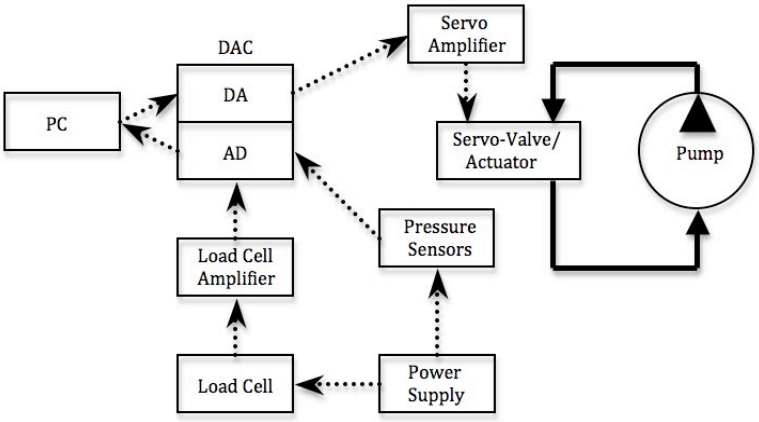

Fig. 4. Block diagram of the hydraulic servo system (dotted and bold arrows represent electric and hydraulic connections, respectively).

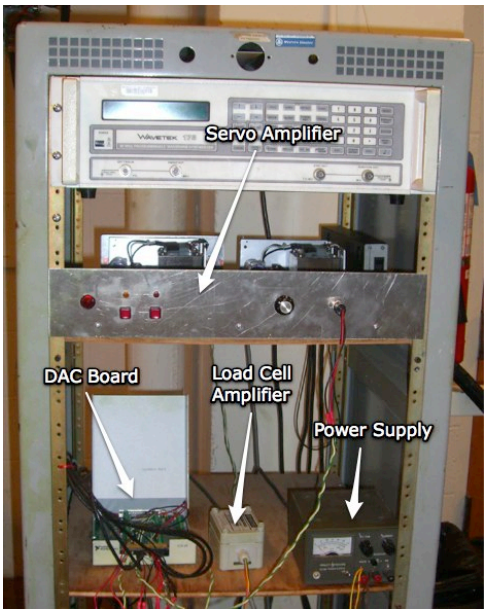

Fig. 5. Electrical equipment.

2.3 Input/Output Characteristics of the System

Increasing the input voltage to the servo-valve amplifier causes an enlarged displacement of the electric actuator within the valve, which results in further movement of the internal spool. The direction the spool moves depends on the sign and/or magnitude of the voltage signal. As the spool displacement increases, the pressure difference between side *A* and *B* of the piston rises. The amount of flow through the needle valve, which is regulated by the open area within the valve, allows a percentage of the pressure between side *A* and *B* to equalize (i.e. the needle valve works to reduce the pressure difference within the actuator). Dividing the pressure difference by the piston area results in the output force magnitude of the actuator (i.e. Force = Pressure/Area). Therefore, with a constant needle valve opening, a given input voltage to the servo-valve corresponds to a specific output force from the actuator.

The open area (cross-sectional area) inside the needle valve has a direct correlation to the volumetric flow rate, Q, through the valve. The needle valve behaves as an orifice. The flow rate through an orifice is given as

$$Q = A_o C_d \sqrt{\frac{2}{\rho}\Delta p}, \tag{1}$$

where A_o is the cross-sectional area within the needle valve, C_d is the discharge coefficient (constant), ρ is the fluid density (assumed to remain constant), and Δp is the pressure difference across the orifice (i.e. the pressure difference between side A and B of the actuator). Increasing A_o or Δp will increase the flow rate through the valve. As fluid flows from the high to low pressure side of the actuator, the pressure difference is reduced, which reduces the magnitude of the output force. Therefore, the relationship between input voltage and output force is dependent on A_o. As A_o increases, a larger pressure can be equalized within the actuator, which results in a smaller force. Therefore, in order for the output force to remain constant, the input voltage to the servo-valve amplifier must be increased as A_o is increased.

The hydraulic power unit, shown in Fig. 3, supplies the servo system with a constant P_{su} of 1000 psi. The double-rod actuator has a piston area of 5.23 in^2 on both side A and B. Therefore, the maximum/minimum output force from the actuator is approximately ±5200 lbf. With no leakage (i.e. the needle valve is completely closed), the system achieves the maximum/minimum output force at an input voltage to the amplifier of ±0.25 V, which is small given the servo amplifier has an operational range of ±5 V (as specified by the manufacturer). As stated above, increasing Q changes the relationship between input voltage and output force. Therefore, to increase the voltage

range for experimentation, the needle valve is opened to increase the volumetric flow through the needle valve. The valve is adjusted until an input of ±2 V results in a maximum/minimum output force of ±4800 lbf. When leakage across the actuator is allowed, the pressure difference between side *A* and *B* of the piston is reduced. Thus, the maximum/minimum output force with leakage (±4800 lbf) is less than the maximum/minimum output force without leakage (±5200 lbf).

Chapter 3.

MODELING THE SYSTEM

3.1 Open-Loop Linear Modeling

An OL linear model of the hydraulic system at a given operating point can be found through experimental input-output measurements. The experimental process for attaining a linear model is as follows.

1. Choose an appropriate input voltage signal.
2. Run experiment and record input voltage data to the servo-valve amplifier and output force data from the load cell.
3. Analyze the input-output data using a fast Fourier transformation (FFT) to find a Bode magnitude and phase plot of the system.
4. Once data is collected over a range of frequencies, a transfer function (TF) best representing the OL response of the system can be found.

The simplest way in finding a linear OL model is to choose an input signal that contains a desired range of frequencies. Since an entire frequency range is represented in the input signal, only one experimental test is needed to find a complete OL model of the system. One signal with such a characteristic is called a chirp signal. A chirp signal is a sine wave whose frequency increases with time and whose amplitude remains constant. The user defines the frequency range and run-time of the signal.

A chirp signal with amplitude of 0.5 V and a frequency range from 0 to 150 Hz is sent to the servo-valve amplifier for a period of 200 seconds. Varying the offset of the chirp signal allows the valve to be tested at different operating points. The purpose of

testing at separate operating points is to find a linear model that best represents the system over a range of inputs. Three separate chirp signals with offsets at 0.25, 0, and -0.25 V are used for testing the servo system. Once the experiments are complete, the input and output data are analyzed using a FFT to obtain the Bode magnitude and phase plots shown in Fig. 6 and Fig. 7, respectively (refer to "Chirp Data"). The Matlab® command *fft* is used in calculating the FFT of the experimental voltage and force data. The results for the chirp signals with input offsets at 0.25, 0, and -0.25 V are represented by trial (a), (b), and (c), respectively. The response of the system is negligible at frequencies > 100 Hz; therefore, only data ≤ 100 Hz is considered. As the frequency increases, the range of the experimental data increases (i.e. there is a larger variance or uncertainty associated with data at higher frequencies). Averaging data values at a given frequency with values near that frequency can filter out the variation in the magnitude and phase data, which results in a set of closely packed data points representing the mean of the experimental results (see "Filtered Chirp Data" in Fig. 6 and Fig. 7).

The OL frequency domain performance of the servo system can also be found using standard sine waves. A sine wave with a frequency ≤ 100 Hz and magnitude of 0.5 V is first sent to the servo-valve amplifier. The magnitude and phase lag of the system can then be found by directly comparing the input and output signals. The main drawback of performing such a test is that several experiments are required to obtain the OL response over the desired frequency range. In contrast, the sine test is useful in verifying the data acquisition process used with the chirp signal. A sine test is performed at 8 separate frequencies for each offset defined by trials (a-c). The magnitude and phase results for the sine test are shown as "*" in Fig. 6 and Fig. 7, respectively. The sine test

data is very similar to the filtered chirp signal data in trials (a-c); therefore, the data acquisition process used in obtaining the OL chirp response is considered accurate.

The experimental data can now be used in finding a linear TF that best matches the system characteristics. Selected magnitude, phase, and frequency values from the filtered chirp data are inputted into the Matlab® command *fitsys* to find a TF that best represents the experimental OL frequency domain data (*fitsys* fits frequency response data with a TF of order *n* using frequency dependent weights). It is desired to have a single TF that approximates the frequency domain performance of the system at each operating point (each chirp signal offset). Trial (b) corresponds to the input signal with an offset of 0 V, which is bounded by trails (a) and (c) with offsets of 0.25 and -0.25 V, respectively. Given the nonlinearities that exist in the servo system, models designed at two separate operating points will tend to differ more from one another as the distance between the operating points (offsets) increase. Therefore, a TF designed with data from trail (b), appose to trial (b) or (c), is expected to more closely model the response of the system at all three offsets.

3.2 Transfer Function Models

A 3rd-order, G_3, and 4th-order, G_4, model of the servo system found using data from trial (b) are given as

$$G_3 = \left(\frac{1.705e4(s-445)}{(s^2+365s+1.705e4)(s+445)} \right) DC \tag{2}$$

and

$$G_4 = \left(\frac{(3.283s^2+1352s+2.624e6)(s-2000)}{(s^3+363s^2+6.894e4s+2.624e6)(s+2000)} \right) DC, \tag{3}$$

where *DC* is the DC-gain of the system (the DC-gain is discussed in length in section 3.3). Both models closely match the experimental phase data for each trial over the full range of frequencies (see Fig. 7). Conversely, only G_4 matches the experimental magnitude data over all frequencies (see Fig. 6). At approximately 20 Hz G_3 begins to diverge away from the experimental magnitude results, which suggests that the system behaves as a higher order model (i.e. $n > 3$) at higher frequencies. Nevertheless, G_3 is not discarded given that it is a good representation of the system at lower frequencies.

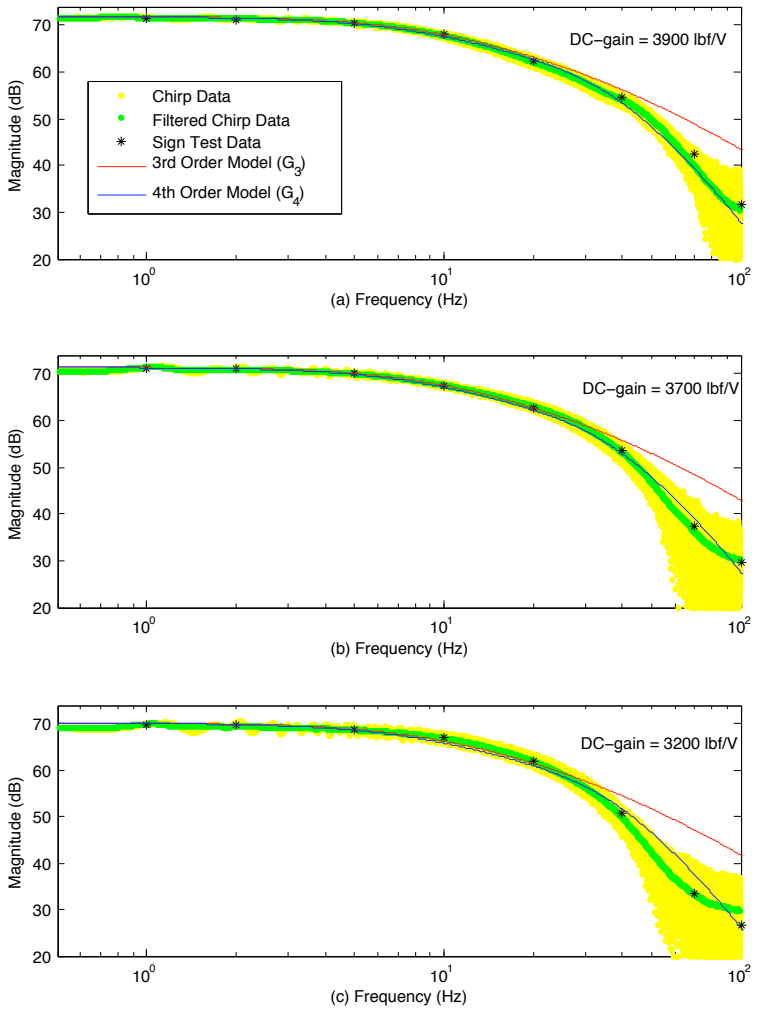

Fig. 6. Bode magnitude of the experimental and analytical results.

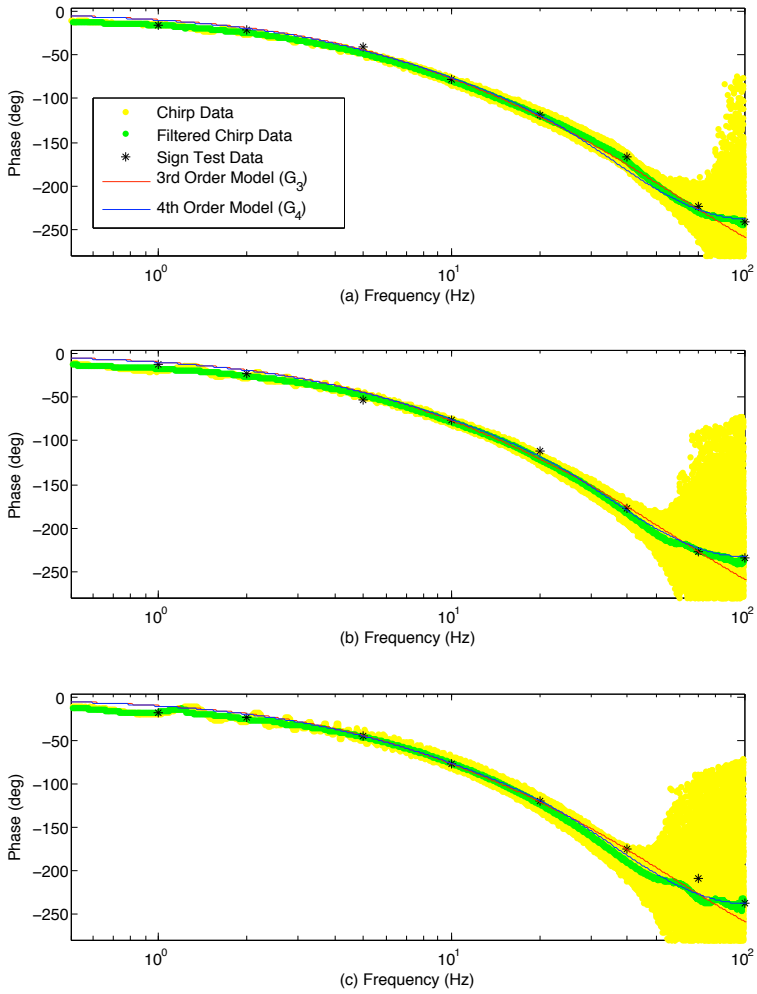

Fig. 7. Bode phase of the experimental and analytical results.

The linear models given in Eqs. (2) and (3) contain a right-half-plane (RHP) zero associated with a 1st-order time delay approximation given as

$$e^{-\theta s} \approx \frac{s - 2/\theta}{s + 2/\theta}, \tag{4}$$

where θ is the time delay in seconds [5]. The time delay for G_3 and G_4 is 4.5 and 1 ms, respectively. The difference in time delay between G_3 and G_4 is due mainly to un-modeled dynamics associated with the 3rd-order model, which influence the time delay approximation (the un-modeled dynamics of G_3 are shown in Fig. 6). Given that G_4 better models the OL response of the system, a time delay of 1 ms is a better

approximation of the real time delay of the servo system. A system with a time delay (i.e. RHP zero) has CL control performance limitations (bandwidth limitations) discussed in Chapter 4.1.

3.3 DC-gain of the Servo System

The DC-gain of the system (represented by *DC* in Eqs. (2) and (3)) corresponds to the change in output force given a change in input voltage (i.e. the slope of output vs. input curve). There are several ways in finding the relationship between the in the input and output of the servo system. The most straightforward procedure is to give the system a constant/static input voltage and record the corresponding output force. This procedure must be repeated over a range of input voltages to acquire an input-output correlation. Depending on the initial voltage of the system, the output force at a given input voltage is found to vary. In other words, the output force at 0 V is different when the system is stepped from -2 to 0 V than when stepped from 2 to 0 V. This inconsistency in the output of a system is referred to as hysteresis. The main cause of hysteresis in the case of a servo-valve is static friction or "stiction" between the moving parts of the valve [1]. One way to reduce stiction is to keep the valve in constant movement by superimposing a dither signal (i.e. a sine wave with given magnitude and frequency) onto the input signal. The magnitude and frequency of the chirp signal must be chosen to keep the stiction within the valve at a minimum without influencing the output force signal.

A second testing procedure for finding an input-output relationship is to give the system a "slow" moving triangular wave over a given range of input voltages (the signal is considered "slow" in that the slope of voltage/time is small). The purpose of using a

slow triangular wave is to define the static relationship between a given input voltage and the resulting output force as the input is increased and decreased. Again, the system has hysteresis resulting from the inconsistencies in the way the system responds as the input voltage is increased (positive slope of the triangular wave) and decreased (negative slope of the triangular wave). Therefore, a dither signal is also applied to the triangular input wave. A dither signal of amplitude 0.4 V and frequency 175 Hz is found to best reduce the valve hysteresis for both the static and triangular tests without affecting the output signal.

The input voltage vs. output force plot for the static and triangular tests are shown in Fig. 8. The static input-output test is performed over an input range from -1 to 1 V at increments of 0.1 V. To limit the number of testing points, the full range of the system is not represented with the static test. For each test voltage, the system is stepped from an initial voltage of ±2 V, which denotes the outer operational bounds of the system. Even with the dither signal superimposed onto the input voltage, the hysteresis of the system is still evident (especially at voltages < -0.5 V). The triangular input-output test is performed over an input range from -2 to 2 V to show the behavior of the DC-gain as the input voltage reaches the outer bounds of the system. The hysteresis magnitude from the triangular test data is significantly lager than from the static test (the output force follows the lower and upper paths as the voltage is increasing and decreasing, respectively). There are also sharp jumps in the force data at input voltages around 1.2 V. These jumps may be a result of the valve sticking and then releasing as the input voltage continues to change.

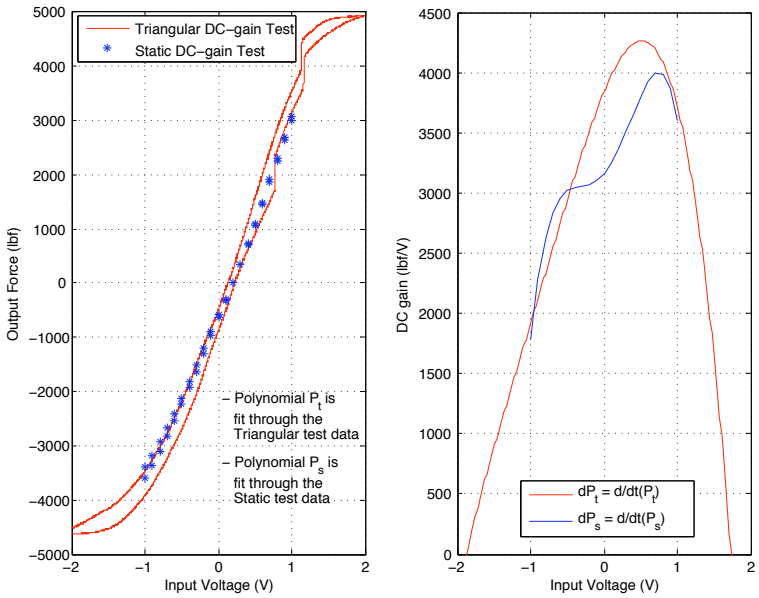

Fig. 8. Output force (left) and DC-gain (right) as a function of input voltage.

Polynomials are fit through the static and triangular data points in Fig. 8 to find an average relationship between force and voltage (P_s and P_t represent the polynomials for the static and triangular input-output tests, respectively). Taking the derivative of P_s and P_t results in polynomials for the DC-gain of the system as a function of input voltage (see DC-gain vs. Input Voltage plot in Fig. 8). Polynomials dP_s and dP_t represent the respective derivatives of P_s and P_t. The DC-gain plots of dP_s and dP_t differ slightly in shape and magnitude, yet their general trends are similar (i.e. they both increase and decrease over similar voltage ranges).

As discussed above, an input of 2 and -2 V results in the maximum and minimum output forces, respectively (i.e. the input range of the system is ±2 V). However, the DC-gain of the system does not remain constant over the entire range of input voltages. As shown in Fig. 8, the DC-gain is a maximum near 0.6 V and decreases as the voltage is increased or decreased. This decline in the DC-gain is mainly due to the leakage across the actuator. As the input approaches the outer bounds of ±2 V, the pressure difference between side *A*

and *B* of the actuator increases. The increased pressure difference causes more fluid to be leaked past the needle valve. This increased flow allows the needle valve to equalize a larger pressure between each side of the actuator, which correlates to a reduction in output force. Therefore, it is expected that the DC-gain of the system (i.e. the slope of the input vs. output curve shown in Fig. 8) will steadily decrease as the input voltage reaches the outer operational bounds. At voltages beyond ±2 V, the system response is insignificant and can be neglected (i.e the DC-gain of the system is near 0).

The average DC-gain values of the system for trials (a-c) are found from the Bode magnitude plots in Fig. 6 (i.e. the magnitude at low frequencies is equivalent to the average DC-gain of the system for each input voltage signal). The average DC-gain can also be found through the use of the DC-gain polynomials, dP_s and dP_t. The *y*-component of a sine wave with the same magnitude and offset as the chirp signals in trials (a-c) is used to evaluate each polynomial. The mean DC-gain output from each polynomial is considered the average DC-gain for the corresponding sine/chirp signal (the frequency of the sine wave has no affect on finding the average DC-gain). Table 1 shows the average DC-gain values of the system and polynomials dP_s and dP_t. As would be expected from the DC-gain plot in Fig. 8, the gain of the system decreases as the input signal offset decreases. Polynomial dP_t is able to reasonably estimate the actual DC-gain of the system. In contrast, polynomial dP_s underestimates the average system gains found in trials (a-c).

Table 1. Average DC-gain values (all values in lbf/V).

	Trial (a) Chirp Offset = 0.25 V	**Trial (b) Chirp Offset = 0 V**	**Trial (c) Chirp Offset = -0.25 V**
System	3900	3700	3200
Static Test (dP_s)	3700	3300	3090
Triangular Test (dP_t)	3960	3720	3360

Polynomial dP_t seems to be an accurate representation of the DC-gain of the system. However, it is found that the DC-gain changes slightly depending on the type, frequency, and magnitude of input voltage signal. For example, if the system is given a sinusoidal input signal, the DC-gain change as the frequency or magnitude of the sine wave is increased of decreased. In addition, the DC-gain behaves in an unpredictable manor when the input signal dynamics increase suddenly (such is the case with a step input). Since the DC-gain polynomials in Fig. 8 are found using input signals with very little dynamics, it is expected that dP_t is more accurate in modeling the DC-gain of the system when the input signal dynamics remain small. Consequently, an accurate representation of the DC-gain is difficult to acquire for a variety of input signals. The uncertainty in the DC-gain is taken into consideration when determining the robust stability/performance of the servo system (see Chapter 6).

Chapter 4.

CONTROLLER DESIGN

4.1 Bandwidth Limitation

The OL models found in Chapter 3.2 contain a RHP zero on the real axis due to the 1st-order time delay approximation; therefore, a bandwidth limitation is placed on the control system. In other words, the performance of a given controller can only be "turned-up" so much before the entire system becomes unstable. For a system with a real RHP zero, z, the achievable bandwidth frequency, ω_B^*, is given as

$$\omega_B^* < z\frac{1-1/M}{1-A}, \tag{5}$$

where M and A are the high and low frequency performance requirements, respectively [5]. Models G_4 and G_3 have respective RHP zeros at 318 and 71 Hz. Setting $M = 3$ (allow 300% error at high frequencies) and $A = 0.1$ (allow 10% error at low frequencies), the maximum achievable bandwidth is found to be 235 Hz for G_4 and 52 Hz for G_3. Since model G_4 better represents the OL response of the servo system (see Fig. 6 and Fig. 7), the approximate time delay corresponding to the RHP zero in G_4 is a more accurate representation of the actual time delay of the system. To achieve the performance requirements given above (i.e. $A = 0.1$ and $M = 3$), a CL bandwidth frequency, ω_B, less than 235 Hz is required. A linear control system with $\omega_B > 235$ Hz will have inadequate performance, and as the bandwidth approaches 318 Hz (i.e. the location of the RHP zero in G_4) the linear system will become unstable. This theoretic bandwidth limitation assumes an entirely linear system, which is not the case when considering the real servo

system. The effects of the nonlinear DC-gain and input saturation on the achievable bandwidth are discussed in Chapter 7.1.

4.2 Controller Overview/Selection

A block diagram of the CL control system is shown in Fig. 9. The control system has the desired force, F_d, as the input and the actual force, F_a, as the output. The output force from the plant, G, is sent as negative feedback (i.e. F_a is subtracted from F_d) resulting in an error signal, e. The error signal is sent thru the controller, K, where it is converted into an appropriate input voltage for G. With no control (i.e. $K = 1$), models G_3 and G_4 are CL instable. In other words, the output of the CL form of each plant exponentially approaches infinity when given an input. This is demonstrated in Fig. 10 with a unit step input.

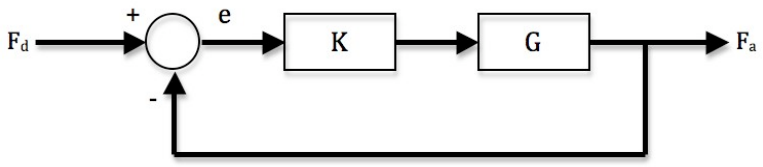

Fig. 9. Block diagram of the closed-loop control system.

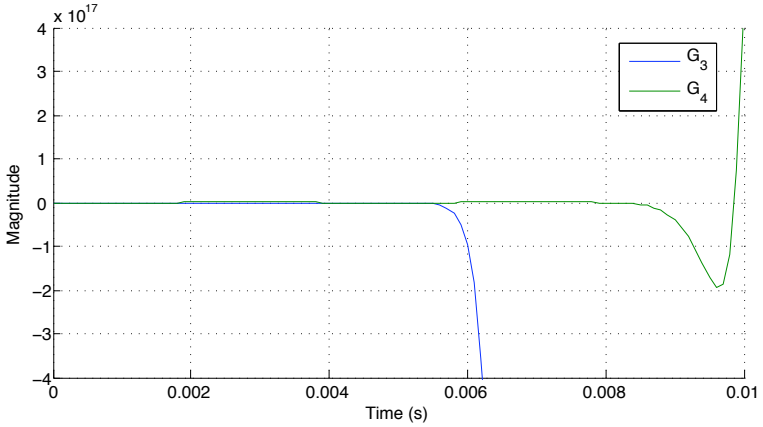

Fig. 10. CL unit step response with no control (i.e. K =1 in Fig. 9).

Four different controllers will be considered to improve the performance of the CL system. The controllers include a Proportional (*P*) controller, a Proportional-Integral-Derivative (*PID*) controller, and two separate H_∞ controllers. A *P* controller, K_P, is the simplest type of controller that can be used for adjusting the input signal to a dynamic system. It works by modifying the error signal, *e*, in Fig. 9 by a factor (i.e. K_P is a constant). For simplicity, consider the classic 2nd order system with a natural frequency, ω_n, and damping ratio, ζ. The error signal for a *P* controlled 2nd-order system is represented by

$$e = \frac{\omega_n^2 F_d}{\omega_n^2 + K_P}. \tag{6}$$

From this equation, the steady-state (SS) error of the system is found to be non-zero, which is an undesirable characteristic in control design. Increasing K_P will reduce the SS error; however, doing so will affect other system dynamics including the un-damped natural frequency and damping ratio [1].

The *PID* controller is expressed in the form

$$K_{PID} = K_P\left(1 + \frac{1}{K_I s} + K_D s\right), \tag{7}$$

where K_I and K_D are the integral and derivative controller gains, respectively. The dynamics of the error signal for a *PID* controlled 2nd-order system are defined as

$$\ddot{e} + \frac{\omega_n^2 + K_P}{2\zeta\omega_n + K_D}\dot{e} + \frac{K_I}{2\zeta\omega_n + K_D}e = 0. \tag{8}$$

For a system at SS, the derivatives of the error, $\ddot{e}$ and $\dot{e}$, go to zero. As a result, the error, *e*, also goes to zero for a *PID* control system. Tuning a *PID* controller can be difficult given that gains K_P, K_I, and K_D have competing effects on the response of the system.

When defining time domain performance, the proportional gain K_P is used to reduce the percent overshoot, the integral gain K_I is used to reduce rise time, and the derivative gain K_D is used to increase stability of the system [1]. A balance between each gain is needed to achieve the desired performance requirements. Controller gains of K_P = 1.2e-3, K_I = 3.0e-3, and K_D = 2.5e-2 are found to provide models G_3 and G_4 with the best overall CL performance (both the *P* and *PID* control systems use these gain values).

To increase the robustness of a control system (i.e. increase the ability of the control system to adjust to uncertainties), H_∞ loop-shaping design is performed to find a controller that optimally robustifies a shaped plant. A shaped plant is a linear model multiplied by some type of controller. For example, a model *G* and controller *K* can be combined into the shaped plant *KG*. The controller within the shaped plant "determines such overall characteristics as response speed, damping characteristics, and steady-state error" of the CL system, while the H_∞ controller is used to compensate for uncertainties [6]. Through the loop shaping procedure, the H_∞ controller, K_H, is defined as

$$K_H = \left[\frac{A + BF + \gamma^2 (L^T)^{-1} Z C^T (C + DF)}{B^T X} \middle| \frac{\gamma^2 (L^T)^{-1} Z C^T}{-D^T} \right] \tag{9}$$

$$F = -S^{-1}(D^T C + B^T X) \tag{10}$$

$$L = (1 - \gamma^2) I + XZ, \tag{11}$$

where *A*, *B*, *C*, *D* is the state-space representation of the shaped plant, Z and X are unique positive definite solutions to the Riccati equations

$$(A - BS^{-1}D^T C)Z + Z(A - BS^{-1}D^T C)^T - ZC^T R^{-1} CZ + BS^{-1}B^T = 0 \tag{12}$$

$$(A - BS^{-1}D^T C)^T X + X(A - BS^{-1}D^T C) - XB^T S^{-1} B^T X + C^T R^{-1} C = 0 \tag{13}$$

and

$$\gamma > \gamma_{\min} = (1 + \rho_s(XZ))^{1/2}, \tag{14}$$

where ρ_s is the spectral radius (maximum singular value) of the shaped plant [5]. The Matlab® M-file *coprimeunc* given by [5] uses the robust control toolbox along with Eqs. (9-14) in obtaining an optimal H_∞ controller for a given shaped plant. Controller K_{PID} and the linear models G_3 and G_4 are used in finding two separate H_∞ controllers (i.e. $K_{PID}G_3$ and $K_{PID}G_4$ are the shaped plants from which the H_∞ controllers are designed). The controllers are given as

$$K_{H3} = \frac{229.7s^2 + 1.334e5s + 6.305e6}{s^3 + 972.4s^2 + 3.579e5s + 1.49e7} \tag{15}$$

and

$$K_{H4} = \frac{231.9s^2 + 7.484e4s + 9.687e6}{s^3 + 601.7s^2 + 1.993e5s + 2.068e7}, \tag{16}$$

where K_{H3} is the H_∞ controller found from the shaped plant $K_{PID}G_3$ (shaped plant containing the 3rd order model) and K_{H4} is the H_∞ controller found from the shaped plant $K_{PID}G_4$ (shaped plant containing the 4th order model).

The robustifying characteristics of the H_∞ controllers can be observed by comparing the OL frequency response of the shaped plants, $K_{PID}G_3$ and $K_{PID}G_4$, with the OL response of the shaped plants with H_∞ control, $K_{H3}K_{PID}G_3$ and $K_{H4}K_{PID}G_4$ (see Fig. 11). The crossover frequency (i.e. the frequency at which the magnitude of the OL response crosses 0 dB) and the phase lag at the crossover frequency for each OL response is given in Table 2. A large OL crossover frequency is representative of a system with a large CL bandwidth frequency, and vice-versa. A system with a large bandwidth has better performance, while a system with a small bandwidth has increased robustness/stability [5]. The OL phase lag at the crossover frequency also gives insight

into the CL stability of the control system. The closer the phase lag is to 180 degrees, the closer the system is to instability [5]. Given these definitions along with the data in Table 2, the *PID* controller is expected to provide better CL performance, and the H_∞ controllers are expected to increase the robustness of the system. The CL performance and stability of each control system is discussed in detail in Chapters 5 and 6.

Table 2. Crossover frequencies and corresponding phase lags for the shaped plants and shaped plants with H_∞ control.

	Crossover Freq. (Hz)	**Phase at Crossover Freq. (deg)**
$\boldsymbol{K_{PID}G_3}$	28.1	128.8
$\boldsymbol{K_{H3}K_{PID}G_3}$	11.9	109.8
$\boldsymbol{K_{PID}G_4}$	25.6	125.5
$\boldsymbol{K_{H4}K_{PID}G_4}$	11.3	107.4

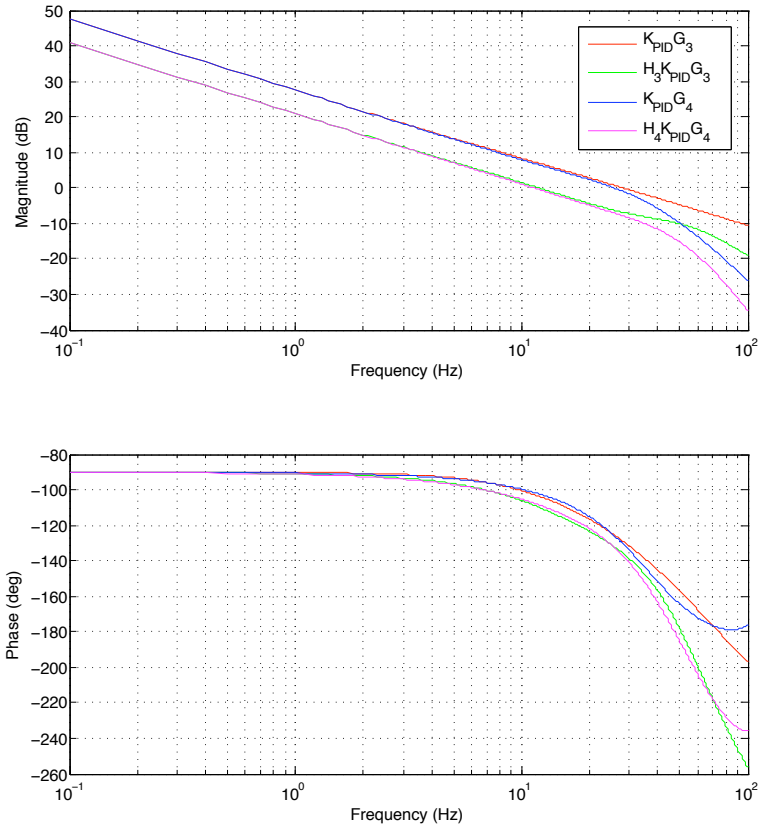

Fig. 11. OL frequency response of the shaped plants and shaped plants with H_∞ control.

Chapter 5.

CLOSED-LOOP PERFORMANCE

5.1 Time Domain Performance

The time domain performance is found by analyzing the response of the CL control system to a step input. Definitions of the time domain performance characteristics are given below for a unit step input.

- **Rise time (t_r)**: the time it takes the output to reach 90% of its final value.
- **Settling time (t_s)**: time after which the output remains within ±2% of its final value.
- **Overshoot**: the peak value divided by the final value.
- **Steady-state error**: the difference in the input and output as time goes to infinity.

For comparing the time domain performance of the system and models with each control system, a step signal with magnitude of 2000 lbf will be used. The desired force signal (F_d in Fig. 9) steps from -1000 to 1000 lbf and then back down to -1000 lbf. The result is a step response for both an increasing and decreasing force. The step response of the system and models with *P*, *PID*, and H_∞ control are given in Fig. 12, Fig. 13, and Fig. 14, respectively. The step response of the system with each control system is shown in Fig. 15 (this figure is used for comparing of the response of each control system). As stated in Chapter 3.1, the DC-gain as a function of input voltage is difficult to predict for input signals with fast changing dynamics, such as a step input, and is therefore assumed to be constant (i.e. *DC* in Eqs. (2) and (3) is constant). The input voltage is bounded between ±2 V. At any voltage beyond ±2 V, the response/gain of the system is

considered insignificant (see Chapter 3.3). It is found that a DC-gain of 3100 lbf is a reasonable approximation for the step input given above.

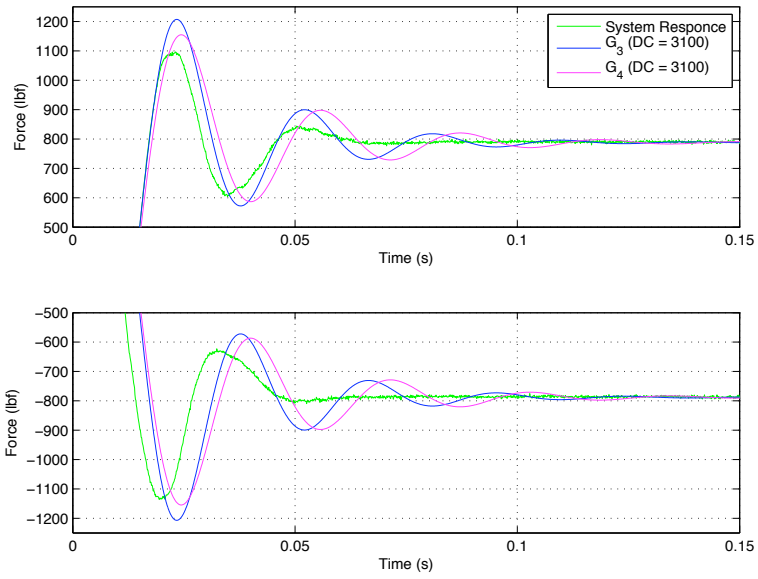

Fig. 12. CL response of the *P* control systems with a reference step input from -1000 to 1000 lbf (top) and 1000 to -1000 lbf (bottom).

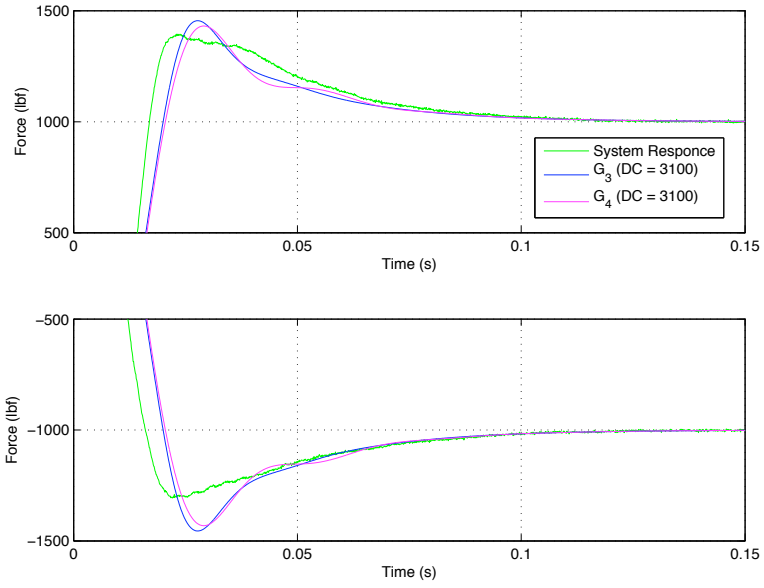

Fig. 13. CL response of the *PID* control system with a reference step input from -1000 to 1000 lbf (top) and 1000 to -1000 lbf (bottom).

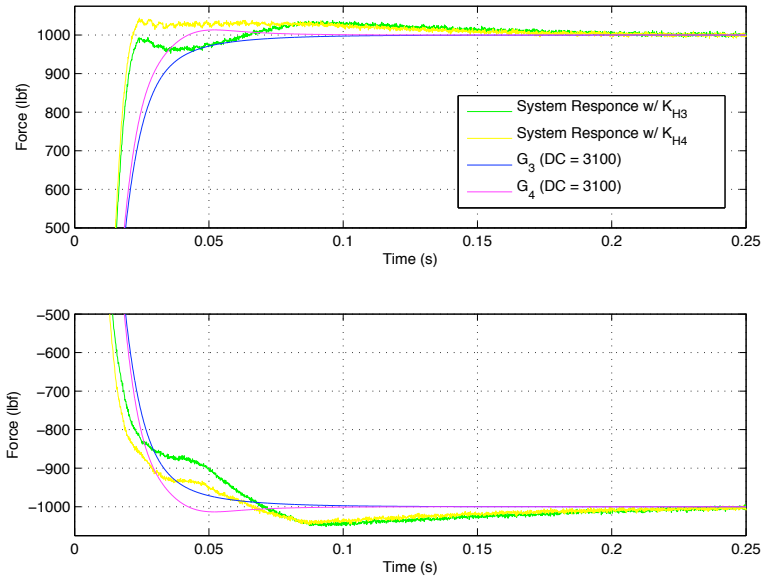

Fig. 14. CL response of the H_∞ control systems with a reference step input from -1000 to 1000 lbf (top) and 1000 to -1000 lbf (bottom).

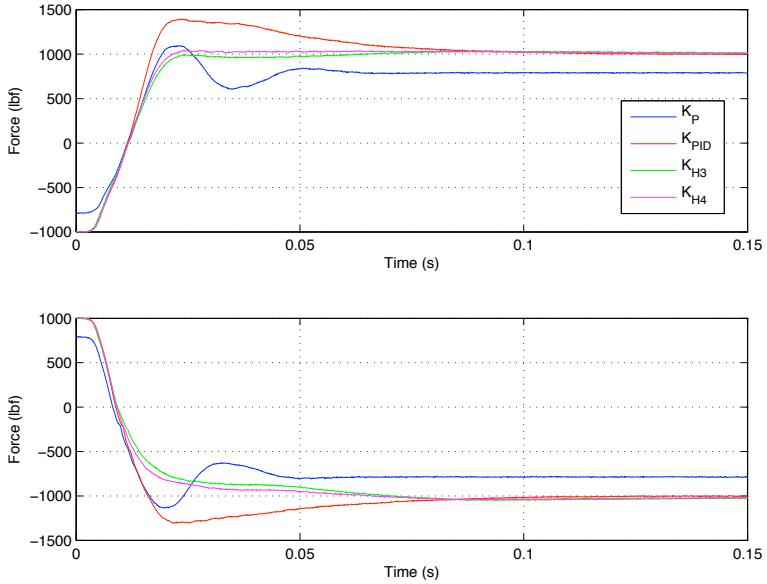

Fig. 15. CL response of the system with a reference step input from -1000 to 1000 lbf (top) and 1000 to -1000 lbf (bottom).

The system and models have an under-damped oscillatory response with SS error when controller K_P is used (see Fig. 12). When comparing the response of the system and models, the settling time of the system is much faster. In addition, the system has a faster rise time when the input signal steps down from 1000 to -1000 lbf. Models G_3 and

G_4 also differ slightly from one another. Model G_4 has less of an overshoot, while G_3 has a faster rise time. Both models have similar settling times. The response of the system and models with controller K_{PID} is also under-damped with an increase in overshoot; however, there is little-to-no oscillation and zero SS error (see Fig. 13). Both the rise time and overshoot of the system are smaller than either model, yet the settling times are very similar for all cases. Models G_3 and G_4 differ in similar ways as they did for the P controlled step response. When the H_∞ controllers, K_{H3} and K_{H4}, are used (see Fig. 14), the response of the system and models has zero SS error and very little overshoot/oscillation (i.e. the damping ratio is close to 1). The system is found to have a much larger settling time and slightly larger overshoot than either model. The system and model G_4 are slightly under-damped (small overshoot), while model G_3 is over-damped (zero overshoot). Given that the H_∞ controllers are designed specifically for G_3 and G_4 (i.e. K_{H3} is designed for G_3 and K_{H4} is designed for G_4), K_{H3} is not be used to control G_4 nor is K_{H4} used to control G_3.

The variations between the time domain response of the system and models described above are mainly due to the assumption of a constant DC-gain. In reality, the gain of the system is continually changing as the input voltage to the servo-valve amplifier changes, which will change the response of the system (this is a non-linear trait of the system). The time domain performance characteristics for all step response data are given in Table 3. The system has a small rise time, settling time, and overshoot with K_P as the control system; however, the SS error associated with P control is a major drawback. Using K_{PID} reduces the rise time and eliminates the SS error, but the settling time and overshoot are increased significantly. The H_∞ controllers also eliminate SS error

and have much smaller overshoots than the other control systems. Then again, they also have the largest rise time and settling time. The frequency domain performance can now be found to more fully understand the performance characteristics of each control system.

Table 3. Time domain performance for system and models.

		Rise Time (ms)	Settling Time (ms)	Overshoot (%)	SS error (%)
P Control (K_P)	**System**	17.1	56.4	6.1	10.6
	G_3	16.6	71.3	9.8	10.6
	G_4	16.5	89.0	13.1	10.6
PID Control (K_{PID})	**System**	15.8	89.1	19.7	0
	G_3	18.4	80.8	22.8	0
	G_4	18.7	82.1	21.6	0
H_∞ Control (K_{H3} and K_{H4})	**System w/ K_{H3}**	18.6	96.1	1.9	0
	System w/ K_{H4}	17.8	91.7	2.2	0
	G_3 w/ K_{H3}	26.6	44.8	0	0
	G_4 w/ K_{H4}	24.4	34.2	0.8	0

5.2 Frequency Domain Performance

The frequency domain performance is characterized via the CL bandwidth frequency, ω_B, of the system. The bandwidth of a system is the frequency range over which control is effective, and the maximum frequency in this range is called ω_B. The bandwidth frequency is very important for understanding the "benefits and trade-offs" for a given feedback control system [5]. Large bandwidths usually correspond to a faster response (i.e. faster rise times and settling times) since high-frequency input signals are more easily passed on to the outputs of the system. Consequently, systems with large bandwidths are also more susceptible to noise or uncertainties in the system. Small bandwidths correspond to a slower response with an increased ability to adjust to uncertainty (i.e. an increased robustness). The CL ω_B is defined as the frequency at which the Bode magnitude plot of the system decreases by 3 dB (the magnitude at low

frequencies is considered the reference frequency). As the magnitude decreases by more than 3 dB, feedback is no longer effective in improving the performance of the system [5].

The control systems found in Chapter 4.2 are designed using the linear TF's found from the OL chirp signal data in Chapter 3.2, more precisely trial (b), which corresponds to an input chirp signal of magnitude 0.5 V and offset of 0 V. The OL response to this chirp signal is shown in Fig. 16 (a time interval of 10 seconds and frequency range of 50 Hz is used). At low frequencies, the OL chirp signal results in a force output magnitude of approximately 1850 lbf at an offset of -400 lbf. To have an accurate comparison of the OL and CL systems, the desired force signal (chirp signal) for each CL control system will have a magnitude and offset equal to the low frequency OL output (i.e. F_d in Fig. 9 is set as a chirp signal with magnitude of 1850 lbf and offset of -400 lbf). Bode magnitude and phase plots for each CL control system can be found through the same process outlined in Chapter 3.1 for the OL system. For easy comparison to the CL control cases, the OL Bode magnitude response is normalized (i.e. the magnitude response is divided by the low frequency gain found from Fig. 6). The full input range of the system (-2 to 2 V) is used in analyzing the CL frequency domain performance to give an overall increase in system performance. The magnitude and phase lag of the normalized OL and CL control cases over a frequency range of 50 Hz are given in Fig. 17 and Fig. 18, respectively. The resulting bandwidth frequencies of the system and models are given in Table 4.

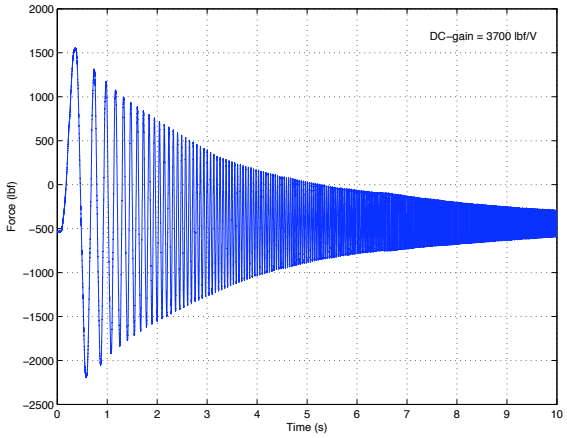

Fig. 16. Open-loop response to a chirp signal with magnitude of 0.5 V, offset of 0 V, and frequency range from 0 to 50 Hz.

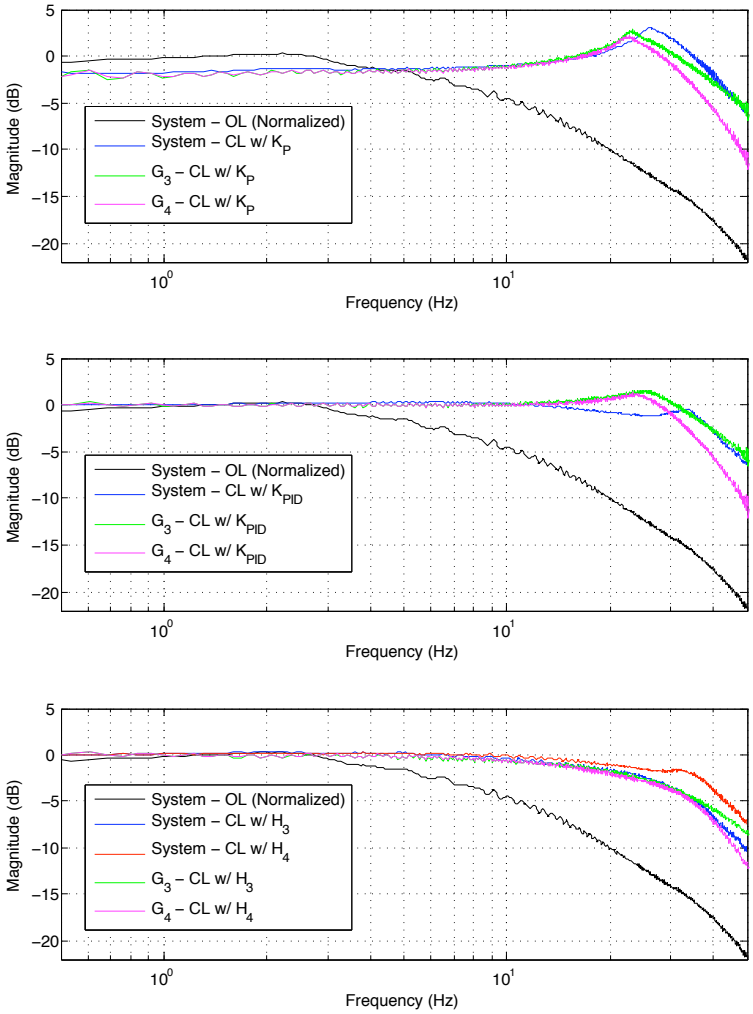

Fig. 17. Bode magnitude plot of the normalized OL and CL *P* control (top), *PID* control (middle), and H_∞ control (bottom) cases.

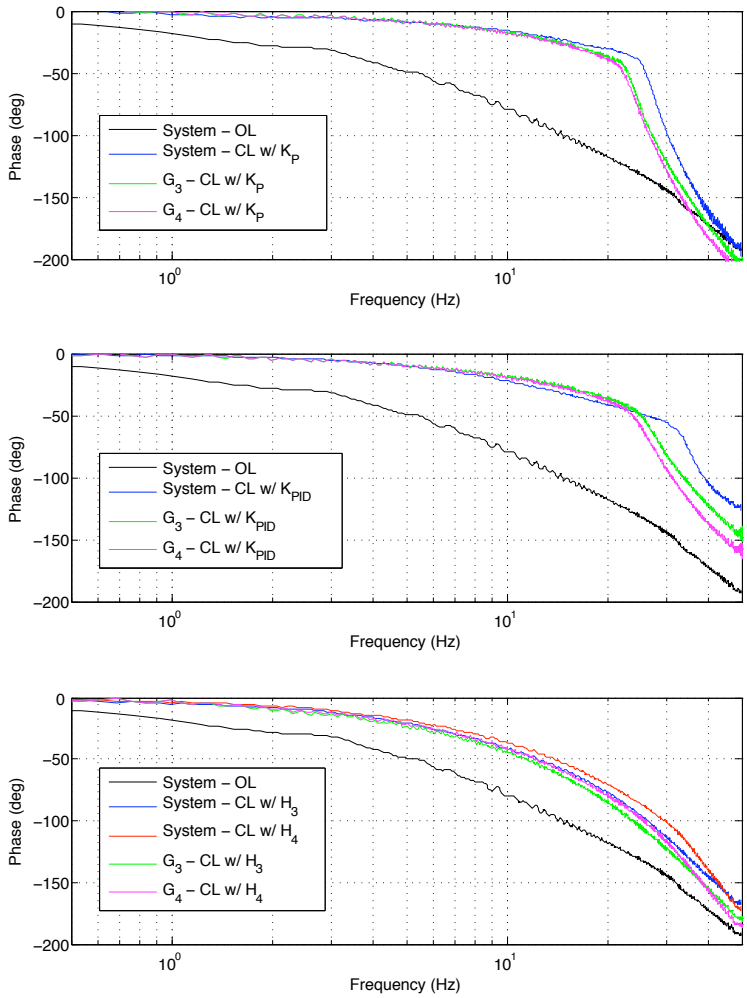

Fig. 18. Bode phase plot of the normalized OL and CL *P* control (top), *PID* control (middle), and H_∞ control (bottom) cases.

As shown in Fig. 17, the CL magnitude response of the system and model G_4 have very similar slopes at higher frequencies, which is most evident with *P* and *PID* control. The CL magnitude response of model G_3 has a smaller slope at higher frequencies due to the inaccuracy of the 3rd-order model in the OL magnitude response (see Fig. 6). The phase plots of the system and models (shown in Fig. 18) all have similar slopes at higher frequencies due to the OL phase accuracy of both models (see Fig. 7). The main differences between the frequency domain response of the system and models are the resonant frequencies for the magnitude (i.e. the frequency at which the

system oscillates at a maximum amplitude) and the drop-off frequencies for the phase (i.e. the frequency at which the phase begins to decrease at an accelerated rate). Both the resonance and drop-off frequencies are smaller for the models than they are for the system. These differences can once again be attributed to the assumption of a constant DC-gain. In fact, the gain of the system is continually changing as the frequency and magnitude of the input voltage to the servo-valve amplifier changes (the gain changes with magnitude due to the gain nonlinearities).

As shown in Table 4, the servo system has bandwidths from largest to smallest with controllers K_P, K_{PID}, K_{H4}, and K_{H4}, respectively. Therefore, controller K_P and K_{PID} provide the system with a faster response (better performance), which corresponds to faster rise times in the time domain (see Table 3). In contrast, controllers K_{H4} and K_{H4} increase the stability of the system (better robustness), which corresponds to small overshoots in the time domain. The saturation frequency of the system and models (i.e. the frequency at which the input voltage reaches ±2 V) is also noted in Table 4 for each CL control system. Decreasing the magnitude of the CL chirp signal (desired force signal) will decrease the amount of saturation the system experiences. However, for sake of comparing the OL and CL responses, reducing the CL chirp magnitude requires an OL response with a smaller output force magnitude (i.e. the OL chirp input voltage magnitude must be reduced).

The only controller that does not cause the system to saturate is K_{H3}, which is also the controller that results in the smallest CL bandwidth. Control systems with small bandwidths do not have the tendency to amplify the error signal as much as higher bandwidth systems (i.e. they are less likely to saturate as the error signal increases in

magnitude). The input voltage to the servo-valve amplifier for CL control with K_{H3} and K_{H4} is shown in Fig. 19. Controller K_{H3} keeps the input voltage to the servo-valve amplifier within ±1.7 V over the entire frequency range; however, controller K_{H3} saturates at approximately 6.2 seconds (33.3 Hz) and remains saturated as the frequency of the chirp signal continues to increase. Nevertheless, limiting the system between ±2 V does not affect the performance of the system as much as one might think. As discussed in Chapter 3.3, the DC-gain of the system gets very small as the input voltage reaches ±2 V. This means that the system does not produce a significant response beyond ±2 V. In other words, the response of the system when given an input of 2 V is nearly the same as the response when given an input of 5 V (5 V is the maximum operating voltage of the servo-valve amplifier as specified by the manufacture). Limiting the input voltage by any more that ±2 V will, however, begin to have an effect on the performance of the system.

Table 4. Bandwidth frequencies for the OL and CL frequency response and corresponding saturation frequencies.

		OL	CL w/ K_P	CL w/ K_{PID}	CL w/ K_{H3}	CL w/ K_{H4}
Bandwidth Freq. (Hz)	**System**	6.9	46.4	40.5	28.2	38.1
	G_3	8.5	46.8	41.1	26.6	-
	G_4	7.8	38.1	34.4	-	25.9
Saturation Freq. (Hz)	**System**	-	32.5	15.1	>50	33.3
	G_3	-	21.3	21.2	>50	-
	G_4	-	20.8	21.3	-	34.1

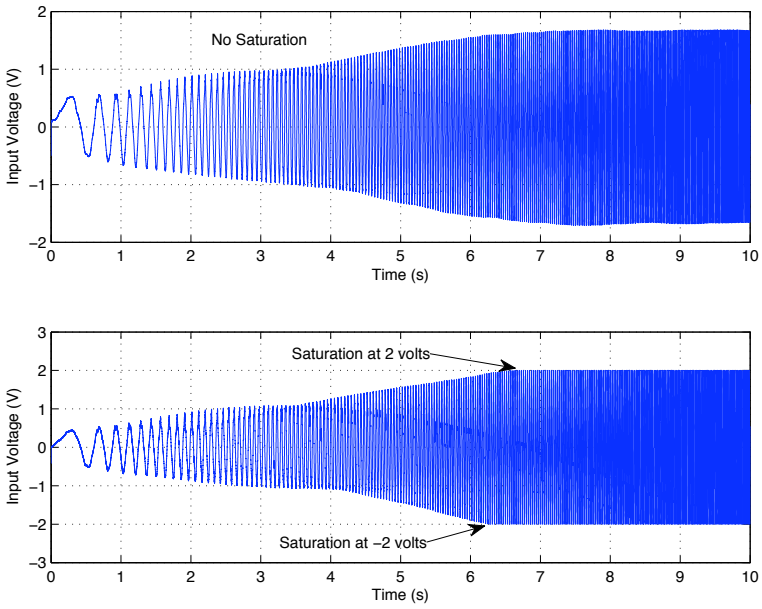

Fig. 19. Input voltage to the servo-valve amplifier for CL control with $K_{H\#}$ (top) and $K_{H\#}$ (bottom).

Chapter 6

NOMINAL/ROBUST STABILITY AND PERFORMANCE

6.1 Dynamic and Parametric Uncertainties

The basic requirement of CL control systems is to achieve a certain level of performance along with the ability to tolerate uncertainties within the system. The performance levels involve such things as "command following, disturbance rejection, [and] sensitivity," while the uncertainty tolerances deal with the "inevitable differences which exist between the physical plant and its mathematical […] model" [7]. Therefore, in order to fully understand a CL control system, it is important to analyze the robustness of the stability and performance characteristics with respect to all plant perturbations [8].

To characterize the stability and performance of each control system, the uncertainties in the system must first be defined. There are two main uncertainties that exist in the servo system: a dynamic (frequency-dependent) uncertainty in the experimental chirp data and a parametric (real) uncertainty in the DC-gain. The dynamic uncertainty is represented as a multiplicative uncertainty (MU) of the form

$$G_{p,d} = G_n(1 + w_I\Delta_I),\ |\Delta_I(j\omega)| \le 1\ \forall\omega \tag{17}$$

where $G_{p,d}$ is the dynamically perturbed plant (i.e. the experimental chirp data), G_n is the nominal plant (i.e. the TF model of the system), w_I is a TF used in modeling the dynamic uncertainty, Δ_I is any stable TF such that $\|\Delta_I\|_\infty \le 1$, and ω is the frequency. The dynamic uncertainty TF, w_I, is found from the relationships

$$l_I(\omega) = \max_{G\in\Pi}\left|\frac{G_{p,d}(j\omega) - G_n(j\omega)}{G_n(j\omega)}\right| \tag{18}$$

and

$$\left|w_I(j\omega)\right| \geq l_I(\omega),\ \forall\omega, \tag{19}$$

where l_I is the maximum MU from the chirp data. Since the 4th order model G_4 matches the experimental OL chirp data over the entire frequency range (0 to 100 Hz) it will represent the nominal plant. The MU uncertainty from each chirp signal (trial (a-c)) is shown in Fig. 20. As defined in Eq. (19), the magnitude of w_I must be greater than or equal to l_I over all frequencies (i.e. w_I represents the least upper bound of dynamic uncertainty over the entire frequency range). The *fitmag* command in Matlab®, which fits a stable TF with minimum phase to a set of magnitude data points, is used in finding a 3rd-order TF, w_I, that bounds all dynamic uncertainties associated with the experimental chirp data (see Fig. 20). The TF form of w_I is defined as

$$w_I = \frac{8.892s^3 + 7825s^2 + 6.49e6s + 1.304e9}{s^3 + 5254s^2 + 1.553e6s + 2.231e9}. \tag{20}$$

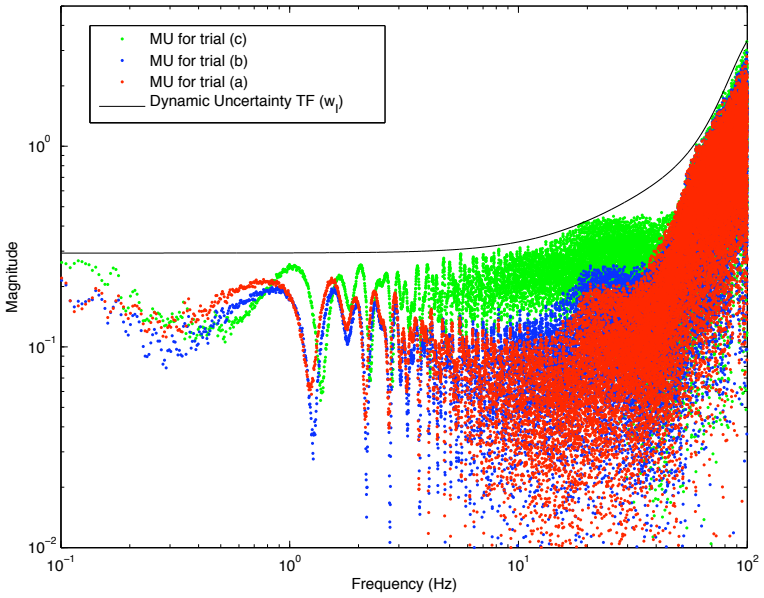

Fig. 20. Dynamic MU for trials (a-c) and resulting uncertainty TF.

The parametric gain uncertainty in MU form is written as

$$G_{p,p} = G_n(1 + r_k\Delta),\ |\Delta| \le 1, \tag{21}$$

where $G_{p,p}$ is the parametrically perturbed plant, Δ is a real scalar, and r_k is the relative magnitude of the gain uncertainty defined by

$$r_k = \frac{(k_{\max} - k_{\min})}{(k_{\max} + k_{\min})}, \tag{22}$$

where k_{max} and k_{min} are the maximum and minimum gain values, respectively. As shown in Chapter 3.3, the input voltage range affects the minimum and maximum DC-gain of the system. Three separate input voltage ranges (±2, ±1, and ±0.5 V) are used to show how changing the input range influences the robust stability/performance of the control systems. Referring to polynomial dP_t in Fig. 8, input ranges of ±2, ±1, and ±0.5 V result in minimum/maximum gains of 0/4250, 1930/4250, and 3420/4135 lbf/V, respectively. Therefore, the relative gain uncertainty magnitude, r_k, for the respective input ranges is 1 (100%), 0.379 (37.9%), and 0.095 (9.5%). Reducing the input range reduces the amount of parametric uncertainty; however, doing so will limit the performance of the system.

6.2 Performance Weight

A block diagram of the servo system with both dynamic and parametric uncertainties is shown in Fig. 21 (G_p is the plant perturbed by both dynamic and parametric uncertainties). To analyze the performance of the system, a performance weight TF, w_P, is also needed. The performance weight is written as

$$w_P = \frac{s/M + \omega_{BR}}{s + \omega_{BR}A}, \tag{23}$$

where M is the allowable error at high frequencies, A is the allowable error at low frequencies, and ω_{BR} is the approximate bandwidth requirement. The inverse of w_P (shown in Fig. 22 for $A = 0.1$, $M = 3$, and $\omega_{BR} = 5$ Hz) represents the upper bound of the sensitivity, $|S|$. The sensitivity function, S, is the TF between the reference input and error in Fig. 21 given as

$$S = \frac{1}{1 + G_p K}. \tag{24}$$

In order for the system to meet the performance requirements defined by w_P, the H_∞ norm of the weighted sensitivity function, $w_P S$, must be less than 1 (alternatively, $|S|$ must be less than $1/|w_P(j\omega)|$ to maintain performance) [5]. Referring to Fig. 22, it is shown that $1/|w_P(j\omega)|$ is equal to A (0.1) at low frequencies and M (3) at high frequencies. If A and M are left constant, increasing or decreasing ω_{BR} will affect how much error is allowed at lower frequencies. Since w_P is a 1st-order TF, the slope of $1/|w_P(j\omega)|$ will not change. As a result, changing the value of ω_{BR} will simply slide the graph in Fig. 22 to the left for smaller ω_{BR} values and to the right for larger ω_{BR} values. Therefore, small and large values of ω_{BR} will increase and decrease the allowable error at lower frequencies, respectively. A CL system that is capable of maintaining performance at the largest possible value of ω_{BR}, which correlates to a system that is able to accurately track higher frequency input signals, is desired. In regards to the servo system, locating w_P on the error signal (see block diagram in Fig. 21) allows the performance of the system to be gauged by the difference between desired force input and actual force output. The error signal is fed through the w_P block and a fictitious uncertainty block, Δ_P,

before it is sent back to the input of the system (see Fig. 21). If the magnitude of the error signal is larger than $1/|w_P(j\omega)|$ at a given ω, the servo system does not maintain the specified performance requirements.

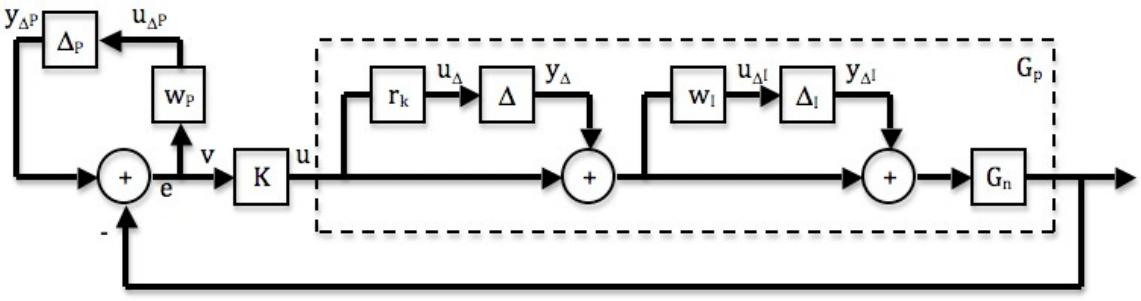

Fig. 21. CL system with multiplicative uncertainties and performance measured at the error.

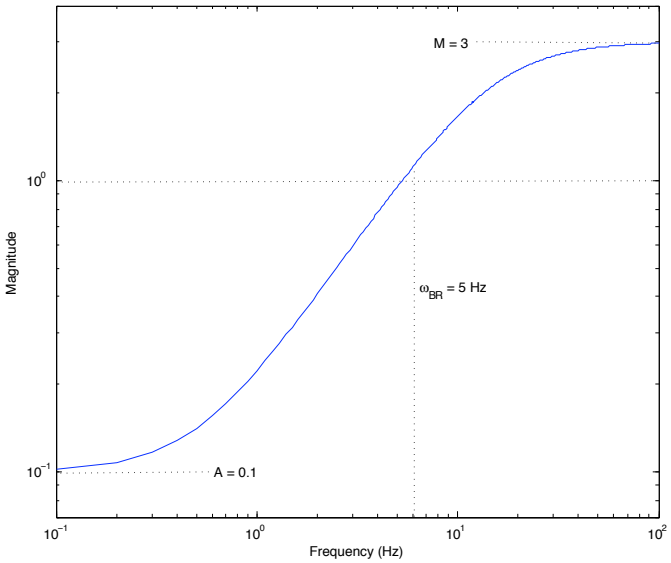

Fig. 22. Inverse of the performance weight (i.e. $1/|w_P(j\omega)|$)

6.3 Obtaining *P* and *N* Matrixes

The Block diagram in Fig. 21 can now be analyzed to obtain the generalized plant model *P*. The generalized plant (shown in matrix form in Fig. 23) contains G_n, w_I, r_k, w_P, and the interconnection structure between the plant and the controller *K* [5]. Referring to

Fig. 21, plant P has u_{Δ}, $u_{\Delta I}$, $u_{\Delta P}$, and v as inputs and y_{Δ}, $y_{\Delta I}$, $y_{\Delta P}$, and u as outputs. The matrix form of P is defined by

$$\begin{Bmatrix} u_{\Delta} \\ u_{\Delta I} \\ u_{\Delta P} \\ v \end{Bmatrix} = [P] \begin{Bmatrix} y_{\Delta} \\ y_{\Delta I} \\ y_{\Delta P} \\ u \end{Bmatrix} \tag{25}$$

$$P = \begin{bmatrix} 0 & 0 & 0 & r_k \\ w_I & 0 & 0 & w_I \\ -w_P G_n & -w_P G_n & w_P & -w_P G_n \\ -G_n & -G_n & 1 & -G_n \end{bmatrix}, \tag{26}$$

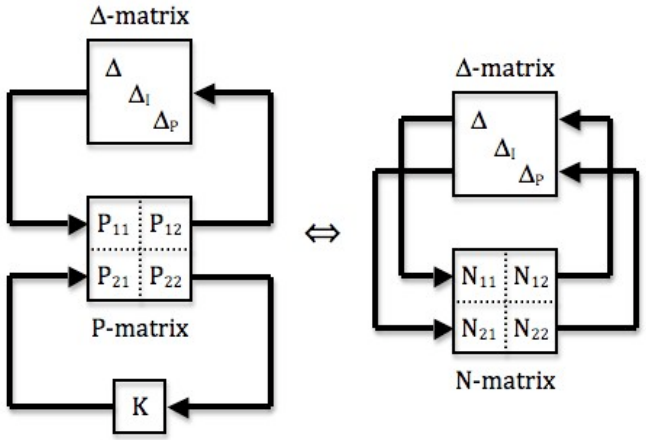

Fig. 23. P and N matrixes.

As shown in Fig. 23, the P-matrix is partitioned into 4 elements (P_{11}, P_{12}, P_{21}, and P_{22}). The column partition corresponds to the number of exogenous inputs from the uncertainty Δ-matrix and the row partition corresponds to the number of endogenous outputs to the uncertainty Δ-matrix. That is to say, P_{11} has dimensions $a \times b$, where a and b are the number of outputs and inputs of the Δ-matrix, respectively. The partitioned elements of P are

$$P_{11} = \begin{bmatrix} 0 & 0 & 0 \\ w_I & 0 & 0 \\ -w_P G_n & -w_P G_n & w_P \end{bmatrix} \quad P_{12} = \begin{bmatrix} r_k \\ w_I \\ -w_P G_n \end{bmatrix} \tag{27}$$

$$P_{21} = \begin{bmatrix} -G_n & -G_n & 1 \end{bmatrix} \quad P_{22} = \begin{bmatrix} -G_n \end{bmatrix}. \tag{28}$$

The controller K can be absorbed into the interconnection structure to obtain the system N. In other words, N is found by using K to close the lower feedback loop around P (see Fig. 23). The equation used in finding the N-matrix from the partitioned P-matrix and controller K is presented below (this is referred to as the lower linear fractional transformation).

$$N = P_{11} + P_{12}K(I - P_{22}K)^{-1}P_{21} \tag{29}$$

The N-matrix has the same dimension as P_{11} (i.e. 3×3). Similar to the P-matrix, the N-matrix is partitioned into 4 elements (N_{11}, N_{12}, N_{21}, and N_{22}). Element N_{11} has dimensions $i \times j$, where i and j are the respective number of outputs and inputs of the parametric, Δ, and dynamic, Δ_I, uncertainty blocks in the Δ-matrix (N_{11} is 2×2). In contrast, element N_{22} has dimension $k \times w$, where k and w are the respective number of performance outputs and inputs of the performance uncertainty block, Δ_P, in the Δ-matrix (N_{22} is 1x1). Therefore, element N_{11} contains information regarding the uncertainties of the system (i.e. r_k and w_I), while element N_{22} contains the performance requirements of the system (i.e. w_P). The off diagonal elements N_{12} and N_{21} may contain uncertainty and/or performance information. The N matrix can now be used in determining the stability and performance of the system.

6.4 Defining Stability/Performance and the Structured Singular Value

The definitions of nominal/robust stability and performance are given below.

- **Nominal stability (NS)**: The system (i.e. nominal model) is stable with no uncertainty. NS $\Leftrightarrow$ N is internally stable (i.e. all eigenvalues of N are in the left half plane (LHP)) [5].
- **Robust stability (RS)**: The system is stable for all perturbed plants about the nominal model up to a worst-case model uncertainty. RS $\Leftrightarrow$ NS and $\mu_{\bar{\Delta}}(N_{11}(\omega)) < 1 \ \forall \omega$, where μ is the structured singular value (SSV) and subscript $\bar{\Delta}$ is the structured 2×2 uncertainty matrix that includes Δ and Δ_I ($\bar{\Delta}$ is diagonal is structure) [5].
- **Nominal performance (NP)**: The system (i.e. nominal model) satisfies the performance specification with no uncertainty. NP $\Leftrightarrow$ NS and $\bar{\sigma}(N_{22}(\omega)) < 1 \ \forall \omega$ [5], where $\bar{\sigma}$ is the maximum singular value of the TF.
- **Robust performance (RP)**: The system satisfies the performance specifications for all perturbed plants about the nominal plant up to the worst-case model uncertainty. RP $\Leftrightarrow$ NS and $\mu_{\hat{\Delta}}(N(\omega)) < 1 \ \forall \omega$, where subscript $\hat{\Delta}$ is the structured 3×3 uncertainty matrix that includes Δ, Δ_I, and Δ_P ($\hat{\Delta}$ is diagonal in structure) [5].

The SSV, μ, is a generalization of $\bar{\sigma}$ and ρ_s [5]. In this structure, parametric uncertainties are handled by replacing them with complex parameters when the singular value is used [8]. Doyle [9] first introduced the SSV in 1982 as a way of "dealing with problems of robust stability with respect to […] uncertainty in situations where it is necessary to exploit the structure of the problem to get less conservative conditions" [10]. In other words, the SSV of a complex system is less than or equal to the maximum

singular value of that system. Therefore, defining stability and performance using $\bar{\sigma}$ instead of μ results in a more conservative result. The conservative nature of using $\bar{\sigma}$ in performing robust analysis on a hydraulic servo system is discussed in detail by [11]. The structured singular value of a complex matrix L is defined by [9] as

$$\mu(L) = (\min\{\bar{\sigma}(\Delta) \mid \det(I + L\Delta) = 0\})^{-1} \tag{30}$$

where Δ denotes a set of complex matrices with $\bar{\sigma}(\Delta) \leq 1$. If no structure Δ exists, $\mu(L) = 0$ [10]. If the structure Δ is 1×1 (i.e. L is a single TF), $\mu(L) = \bar{\sigma}(L)$ (this relationship is used in defining NP since N_{22} is a 1×1 TF matrix). A value of $\mu = 1$ signifies that there exists a perturbation just large enough to make $I + L\Delta$ singular (feedback is no longer considered effective when $\mu > 1$). A larger value of μ (say 0.99) requires only a smaller perturbation to make $I + L\Delta$ singular; therefore, smaller values of μ are desired [5]. An algorithm by [12] dating back to 1986 uses "several smooth optimization problems" to solve for μ. For simplicity, the Matlab® command *ssv* is used for all SSV calculations.

6.5 Nominal and Robust Stability

The stability of the servo system is tested for input voltage ranges of ±2 V (r_k = 1), ±1 V (r_k = 0.379), and ±0.5 V (r_k = 0.095). The N-matrix for each control system has eigenvalues in the LHP when r_k equals 0.095, 0.379, and 1. Therefore, each controller provides NS to the CL system for input voltage ranges up to ±2 V. The RS of the control systems at each value of r_k is determined through the structured singular values of N_{11} over a frequency range from 0 to 100 Hz (see Fig. 24). All controllers are found to provide RS (i.e. $\mu_{\bar{\Delta}}(N_{11}(\omega)) < 1 \ \forall \omega$) when r_k = 0.095 and r_k = 0.379. However, when r_k

= 1, controllers K_P and K_{PID} are unable to maintain stability for all perturbed plants (i.e. $\mu_{\bar{\Delta}}(N_{11}(\omega)) > 1$ for certain ω values). Small values of $\mu_{\bar{\Delta}}(N_{11}(\omega))$ correlate to system with better RS (i.e. a larger "additional" perturbation is needed to cause $\mu_{\bar{\Delta}}(N_{11}(\omega)) = 1$). As shown in Fig. 24, $\mu_{\bar{\Delta}}(N_{11}(\omega))$ is the smallest for controller K_P at small ω values. Yet, the H_∞ controllers, K_{H3} and K_{H3}, have better RS for any $\omega >$ 10 Hz, which is a result of the robustifying characteristics of H_∞ control (i.e. the H_∞ controllers allow the system to adjust better to uncertainties, especially at higher frequencies). Both K_P and K_{PID} have resonance peaks near 30 Hz that cause the control systems to fail the RS criteria when r_k = 1 (see Fig. 24). These resonance peaks also show up in the CL frequency domain performance plot in Fig. 17. Table 5 gives the NS and RS for each control system.

Table 5. Stability and performance of each control system.

	Controller	NS	RS	NP	RP
Input range ±0.5 V r_k **= 0.095**	K_P	Yes	Yes	Yes ($\omega_{BR} \leq$ 5.2 Hz)	No
	K_{PID}	Yes	Yes	Yes ($\omega_{BR} \leq$18.1 Hz)	No
	K_{H3}	Yes	Yes	Yes ($\omega_{BR} \leq$10.6 Hz)	Yes ($\omega_{BR} \leq$ 6.6 Hz)
	K_{H4}	Yes	Yes	Yes ($\omega_{BR} \leq$11.9 Hz)	Yes ($\omega_{BR} \leq$ 7.4 Hz)
Input range ±1 V r_k **= 0.379**	K_P	Yes	Yes	Yes ($\omega_{BR} \leq$ 5.2 Hz)	No
	K_{PID}	Yes	Yes	Yes ($\omega_{BR} \leq$18.1 Hz)	No
	K_{H3}	Yes	Yes	Yes ($\omega_{BR} \leq$10.6 Hz)	Yes ($\omega_{BR} \leq$ 3.5 Hz)
	K_{H4}	Yes	Yes	Yes ($\omega_{BR} \leq$11.9 Hz)	Yes ($\omega_{BR} \leq$ 2.5 Hz)
Input range ±2 V r_k **= 1**	K_P	Yes	No	Yes ($\omega_{BR} \leq$ 5.2 Hz)	No
	K_{PID}	Yes	No	Yes ($\omega_{BR} \leq$18.1 Hz)	No
	K_{H3}	Yes	Yes	Yes ($\omega_{BR} \leq$10.6 Hz)	No
	K_{H4}	Yes	Yes	Yes ($\omega_{BR} \leq$11.9 Hz)	No

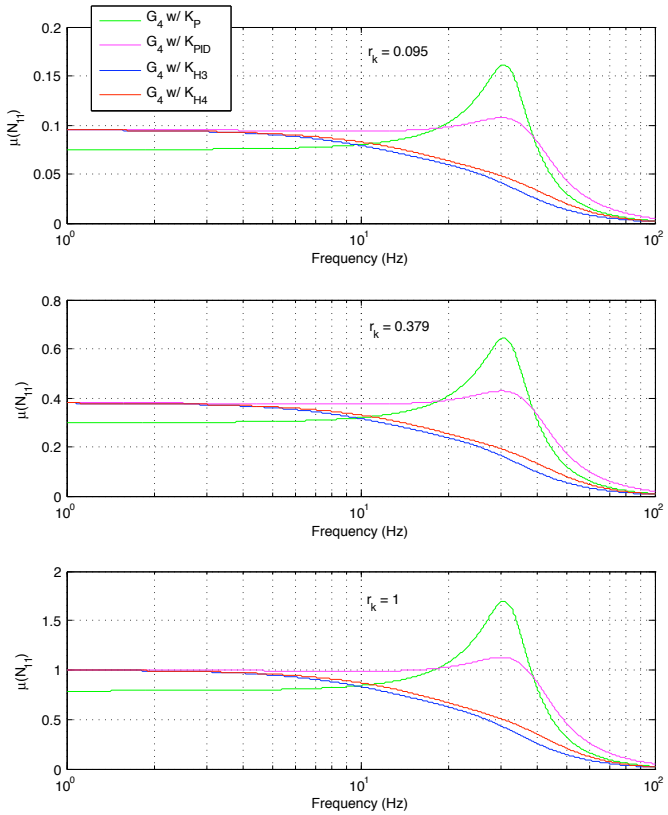

Fig. 24. Robust stability (i.e. $\mu_{\tilde{\Delta}}(N_{11}(\omega)) < 1$) for $r_k = 0.095$ (top), $r_k = 0.379$ (middle) and $r_k = 1$ (bottom).

6.6 Nominal and Robust Performance

The performance is also tested for $r_k = 1$, $r_k = 0.379$, and $r_k = 0.095$. To find the performance of each control system, the performance weight TF, w_P, shown in Eq. (23), must first be defined. Referring to Fig. 21, the performance weight is placed on the error signal; therefore, the magnitude of the error will determine if the system meets the given performance requirements. The allowable errors are set at 10% ($A = 0.1$) for low frequencies and 300% ($M = 3$) for high frequencies (the same values of A and M are used in defining the bandwidth limitation of the system in Chapter 4.1). The performance of each control system is tested at different values of the ω_{BR} (bandwidth requirement) to find at what bandwidth the system is considered to have NP and RP.

A control system with NP up to a given bandwidth is able to provide the nominal plant, G_n, adequate performance (as defined by w_P) up to that bandwidth. For example, a control system that provides G_n with NP up to $\omega_{BR} = x$ Hz is able to effectively track a sine wave at a frequency up to x Hz. The NP (i.e. $\bar{\sigma}(N_{22}(\omega)) \ \forall \omega$) for each control system is illustrated in Fig. 25 for ω_{BR} = 10 Hz. The *PID* controller is shown to have the best NP for any $\omega < 30$ Hz, while the H_∞ controllers have the best NP for any $\omega > 30$ Hz (the NP of the H_∞ controllers increases as ω increases beyond 5 Hz). The *P* controller does not have NP at ω_{BR} = 10 Hz. Once again, K_P and K_{PID} have resonance peaks near 30 Hz that have a negative affect on the NP of the system. Table 5 shows the bandwidths over which each control system maintains NP. Since N_{22} does not contain any uncertainty information, each controller has the same NP for the different values of r_k. Controller K_{PID} is able to provide the system with NP over the largest bandwidth (18.1 Hz). Controller K_P has the smallest NP range (5.2 Hz) given that the SS error associated with *P* control causes the system to exceed the performance requirements at low frequencies (see Fig. 25). The H_∞ controllers have similar NP bandwidths (10 to 11 Hz); however, controller K_{H4} is able to maintain NP for a slightly higher value of ω_{BR}.

To qualify as having RP, the structured singular values of the entire *N*-matrix must be less than one over all frequencies. A control system with RP up to a given ω_{BR} is able to provide the perturbed plant, G_p, with adequate performance up to that bandwidth. Since the N-matrix contains uncertainty and performance information, a system must have a balance between robustness (good RS) and fast response time (good NP) to qualify for RP. For this reason, if a given CL control system does not have RS (i.e.

$\mu_{\bar{\Delta}}(N_{11}(\omega)) > 1$) or NP (i.e. $\bar{\sigma}(N_{22}(\omega)) > 1$), the system will not have RP. Therefore, when the parametric uncertainty for the DC-gain is 100 % ($r_k = 1$), controllers K_P and K_{PID} are automatically disqualified from providing RP. In fact, no control system is able to provide RP when $r_k = 1$. However, both H_∞ controllers do offer RP when $r_k = 0.379$ and $r_k = 0.095$ (see Table 5).

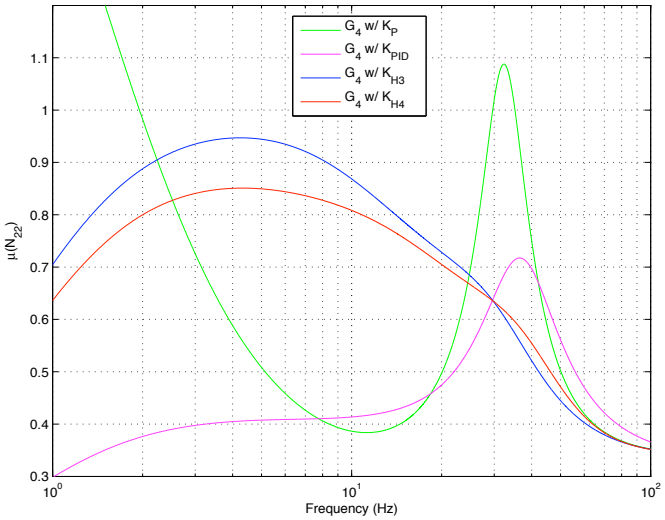

Fig. 25. Nominal performance (i.e. μ (N_{22})) with $A = 0.1$, $M = 3$, and $\omega_{BR} = 10$ Hz.

As shown in Table 5, controller K_{PID} has the best NP frequency range, yet K_{PID} is unable to offer RP given that it has RS issues near 30 Hz caused by the resonance of the *PID* controller (see Fig. 24). Controller K_P does not provide RP given that is has poor NP due to the low frequency SS error of the *P* controller (see Table 5 and Fig. 25). The H_∞ controllers are able to provide RP given that they have excellent RS and decent NP (see Table 5, Fig. 24, and Fig. 25). Limiting the input voltage range of the servo system, which reduces the significance of the parametric uncertainty by limiting the gain of the system, increases the bandwidth range over which the H_∞ controllers maintain RP (see

Table 5). However, by limiting the input voltage, the response of the system will be restricted causing a reduction in the overall performance of the servo system.

Chapter 7.

CONCLUSION

7.1 Experimental Results

The OL response of the hydraulic servo system is best represented as the 4th-order linear TF model, G_4, containing a 1st-order time delay approximation (the 3rd-order TF is unable to model the system at higher frequencies). The RHP zero associated with the time delay places a bandwidth limitation, ω_B^*, of 235 Hz on any feedback control system. In other words, the CL bandwidth, ω_B, of a control system must be less than 235 Hz to meet the performance requirements of $A = 0.1$ (10% error at low frequencies) and $M = 3$ (300% error at high frequencies) (see Eq. (5)). Therefore, there theoretically exists a controller capable of providing G_4 with $\omega_B = 225$ Hz (a high order controller is most likely required to achieve such a bandwidth).

The bandwidth limitation analysis is based on the linear model G_4; therefore, it does not take into account any non-linear behaviors of the real system such as the deterioration of the DC-gain as the input voltage increases or the saturation of the system. Furthermore, the OL magnitude response of the system is found to be insignificant at any frequency greater than 100 Hz (the same cannot be said for the linear model). The actual ω_B^* of the non-linear servo system is, therefore, expected to be at some frequency less than 235 Hz. Of the four controllers designed, the *P* controller, K_P, results in the largest CL bandwidth of 46.4 Hz, which is much smaller than the linear ω_B^*. Modifying each controller (i.e. adjusting controller gains) can further increase the CL bandwidth of the system; however, doing so may have an adverse affect on the performance and/or

robustness of the system. As the overall gain of a controller is increased, the amount of saturation the system experiences will also increase. When the system saturates, the effectiveness (i.e. the performance) of the control system is diminished. As a result, the non-linear characteristics of the servo system cause the actual ω_B^* to be significantly less than what is predicted from the linear model.

When considering time domain performance, K_P and K_{PID} provide the system with the fastest rise times, while K_{H3} and K_{H4} result in the least amount of overshoot. The frequency domain performance results show that controllers K_P and K_{PID} provide the fastest response (i.e. better performance) and controllers K_{H3} and K_{H4} as providing the best stability (i.e. better robustness). Controller K_{H3} is the only controller that does not cause saturation when tracking a chirp signal with magnitude of 1850 lbf, offset of -400 lbf, and frequency range of 50 Hz. The ability of a control system to stay within the active input range of the system (especially at high magnitudes and frequencies) is very desirable.

Controller K_{H3} provides the lowest CL bandwidth frequency (28.2 Hz) of any control system, meaning it is better able to adjust to uncertainties within the system. As a result of this low bandwidth, the RS (i.e. $\mu_{\bar{\Delta}}(N_{11}(\omega))$) of the K_{H3} control system has the smallest magnitude over the majority of the frequency range (see Fig. 24). Controller K_P has the best RS at low frequencies ($\omega < 10$ Hz), but its large resonance peak rear 30 Hz causes its overall RS to be poor.

Controller K_{PID} offers NP up to a bandwidth of 18.1 Hz, while K_{H3} and K_{H4} have NP up to 10.6 and 11.9 Hz, respectively (the performance weight allows 10% error at low frequencies and 300% error at high frequencies). These NP results correlate to the

frequency domain performance results (i.e. the faster the system can respond, the better performance it will have). Generally, a higher CL ω_B will result in a control system with better NP. Yet, K_P results in the highest CL ω_B and poorest NP of all the control systems. This is due to the SS error associated with *P* control (i.e. the SS error causes the system to exceed the low frequency performance criteria at a very small value of ω_{BR}).

In order for the servo system to have RP, the control system must have a balance between performance and stability. The only controllers capable of providing RP are K_{H3} and K_{H4} (see Table 5 for RP data for K_{H3} and K_{H4}). Controller K_{H3} provides better RP for the ±1 V input range (r_k = 0.379), while K_{H4} provides better RP for the ±0.5 V input range (r_k = 0.095). Since decreasing the input range has significant affects on CL performance, it is desired to have a control system with the best possible performance at the largest possible input range. Therefore, it is concluded that the best overall control (i.e. the best balance of CL performance and stability) is attained with K_{H3}.

7.2 Future Work

The force analysis of the system can be investigated further by allowing rod movement during testing. As shown in Fig. 1, the hydraulic actuator rod (rod *A*) is connected to a bracket to eliminate any movement of the actuator rod during loading. To allow for rod movement, a secondary hydraulic actuator can be used to replace the bracket. By adding a leakage line and needle valve to the secondary actuator (similar to what is shown in Fig. 1 for the main loading actuator), the speed at which the actuators move can be regulated by increasing or decreasing the flow through the secondary actuator. Increasing the flow rate between the high and low-pressure side of the

secondary actuator will cause the actuator to be compressed at a faster rate when subjected to a load. To overcome the problems of force control caused by actuator movement, the CL control system (see in Fig. 9) can be modified by adding a correction to the force demand based on the displacement and/or velocity of the main actuator [4]. Allowing movement in the main actuator rod is beneficial in developing a platform for testing other actuators. Such a system is outlined by [4] where primary flight actuators for aircraft are tested by connecting a main loading actuator to a lever arm, which is in turn connected to a secondary flight actuator. By using a similar setup as outlined by [4], along with the control design process outlined in this thesis, a control system with the required performance and robustness can be created for testing a variety of other hydraulic, pneumatic, or electronic actuators.

Further work can also be conducted to improve the bandwidth/performance of the control system. Non-linear QFT robust control methodology given by [2], Input-Output Feedback Linearization given by [3], or a different non-linear approach can be used to improve the robustness of the servo system by compensating for the non-linear gain curve shown in Fig. 8. Non-linear procedures are more involved than the linear process outlined in this thesis, but they should result in a control system that is better able to compensate for the non-linearities in the servo system and improve upon the overall performance.

BIBLIOGRAPHY

[1] Manring, N. D., 2005, *Hydraulic Control Systems*, John Wiley & Sons, Hoboken, NJ, 61-64, 156-160, 169-176, 234-252.

[2] Niksefat, N., and Sepehri, N., "Robust Force Controller Design for a Hydraulic Actuator Based on Experimental Input-Output Data." IEEE Proc., Vol. 5, Issue 2-4, pp. 3718-3722, 1999.

[3] Chiriboga, J., Thein, M.-W.L., and Misawa, E.A., "Input-Output Feedback Linearization Control of a Load-Sensing Hydraulic Servo System," IEEE Proc., pp. 910-915, 1995.

[4] Rito, G. D., Denti E., and Galatolo R., "Robust Force Control in a Hydraulic Workbench for Flight Actuators," IEEE Proc., Issue 4-6, pp. 807-813, 2006.

[5] Skogestad, S. and Postlethwaite, I., *Multivariable Feedback Control: Analysis and Design*, John Wiley & Sons Ltd, second edition, Feb. 2005, 22, 30, 32-34, 38-39, 56, 60-62, 105-110, 127, 186, 306-319, 364-368.

[6] Lu, H. C., Lin, W. C., "Robust Controller with Disturbance Rejection for Hydraulic Servo System," IEEE Proc., Vol. 40, Issue 1, pp. 157-162, 1993.

[7] Doyle, J. C., Wall, J. E., and Stein, G., "Performance and Robustness Analysis for Structured Uncertainty," IEEE Proc., Vol. 21, Part 1, pp. 629-636, 1982.

[8] Sideris, A., and Sanchez Pena, R. S., "Robustness Margin Calculation with Dynamic and Real Parametric Uncertainty." IEEE Proc., Vol. 35, Issue 8, pp. 970-974, 1990.

[9] Doyle, J. C., "Analysis of Feedback Systems with Structured Uncertainty," IEE Proc., Part D, Vol. 129, pp. 251-256, 1982.

[10] Djukanovic, M., Khammash, M., and Vitta1, V., "Structured Singular Value Theory Based Stability Robustness of Power Systems," IEEE Proc., Vol. 3, Issue 10-12, pp. 2702-2707, 1997.

[11] Cheng, Y., and De Moor, B. L. R., "Robust Analysis and Control System Design for a Hydraulic Servo System," IEEE Proc., Vol. 2, Issue 3, pp. 183-197, 1994.

[12] Fan, M. K. H., Tits, A. L., "Characterization and Efficient Computation of the Structured Singular Value," IEEE Proc., Vol. 31, Issue 8, pp. 734-743, 1986.